Received: 25 June 2022 | Revised: 29 October 2022 | Accepted: 1 November 2022

DOI: 10.1002/pld3.465

ORIGINAL RESEARCH

Opposing effects of *trans*- and *cis*-cinnamic acid during rice coleoptile elongation

Lena Vlaminck[1,2,3] | Brix De Rouck[3] | Sandrien Desmet[4] | Thijs Van Gerrewey[3] | Geert Goeminne[4] | Lien De Smet[5] | Veronique Storme[1,2] | Tina Kyndt[5] | Kristof Demeestere[6] | Godelieve Gheysen[5] | Dirk Inzé[1,2] | Bartel Vanholme[1,2] | Stephen Depuydt[1,2,3]

[1]Department of Plant Biotechnology and Bioinformatics, Ghent University, Ghent, Belgium

[2]VIB-UGent Center for Plant Systems Biology, Ghent, Belgium

[3]Laboratory of Plant Growth Analysis, Ghent University Global Campus, Incheon, South Korea

[4]VIB Metabolomics Core Ghent, Ghent, Belgium

[5]Department of Biotechnology, Ghent University, Ghent, Belgium

[6]Department of Green Chemistry and Technology, Ghent University, Ghent, Belgium

Correspondence
Stephen Depuydt and Bartel Vanholme, VIB-UGent Center for Plant Systems Biology, 9052, Ghent, Belgium.
Email: stephen.depuydt@ghent.ac.kr and bartel.vanholme@ugent.be

Funding information
UGent | Bijzonder Onderzoeksfonds UGent (BOF), Grant/Award Numbers: BOF08/01M00408, BOF01D28016

Abstract

The phenylpropanoid cinnamic acid (CA) is a plant metabolite that can occur under a *trans*- or *cis*-form. In contrast to the proven bioactivity of the *cis*-form (*c*-CA), the activity of *trans*-CA (*t*-CA) is still a matter of debate. We tested both compounds using a submerged rice coleoptile assay and demonstrated that they have opposite effects on cell elongation. Notably, in the tip of rice coleoptile *t*-CA showed an inhibiting and *c*-CA a stimulating activity. By combining transcriptomics and (untargeted) metabolomics with activity assays and genetic and pharmacological experiments, we aimed to explain the underlying mechanistic processes. We propose a model in which *c*-CA treatment activates proton pumps and stimulates acidification of the apoplast, which in turn leads to the loosening of the cell wall, necessary for elongation. We hypothesize that *c*-CA also inactivates auxin efflux transporters, which might cause a local auxin accumulation in the tip of the coleoptile. For *t*-CA, the phenotype can partially be explained by a stimulation of cell wall polysaccharide feruloylation, leading to a more rigid cell wall. Metabolite profiling also demonstrated that salicylic acid (SA) derivatives are increased upon *t*-CA treatment. As SA is a known antagonist of auxin, the shift in SA homeostasis provides an additional explanation of the observed *t*-CA-mediated restriction on cell growth.

KEYWORDS
bioactivity, cinnamic acid, coleoptile elongation, *Oryza sativa*

1 | INTRODUCTION

The phenylpropanoid pathway serves as a source for a large variety of aromatic plant metabolites with a broad range of functions (Agati et al., 2012; Biała & Jasiński, 2018; Fraser & Chapple, 2011; Mathesius, 2018; Vogt, 2010). The main end products of the pathway are the monolignols that are deposited in the apoplast, where they polymerize into lignin (Vanholme et al., 2012; Vogt, 2010). This highly recalcitrant aromatic polymer provides strength and hydrophobicity to the plant cell wall, allowing for an upright growth of terrestrial plants

and assuring long-distance water transport (Chabannes et al., 2001; Jones et al., 2001). Although the majority of carbon that enters the phenylpropanoid pathway is channeled toward these monolignols, many of the pathway intermediates function as branch points directing carbon skeletons to side pathways that lead toward aromatic metabolites such as benzenoids, coumarins, and flavonoids (Vogt, 2010). These secondary metabolites are involved in various physiological processes essential for plant growth and survival, including nutrient uptake, pollinator attraction, protection against UV stress, and defense against pests and pathogens (Agati et al., 2012; Clemens & Weber, 2016; Liu & Murray, 2016; Naoumkina et al., 2010; Shalaby & Horwitz, 2015; Yang et al., 2018).

Several phenylpropanoids not only act as intermediates in a highly complex metabolic network but also trigger a direct response when added to plants (Guaadaoui et al., 2014). Unfortunately, the literature on these so-called bioactive phenylpropanoids is ambiguous (Vanholme et al., 2019). The best characterized bioactive intermediate of the phenylpropanoid pathway is cinnamic acid (CA), which is formed by the deamination of phenylalanine by PHENYLALANINE AMMONIA LYASE (PAL). Like all phenylpropanoids, CA has an unreduced double bond in its side chain and thus can occur as a *trans*- or *cis*-form (i.e. *t*-CA and *c*-CA, respectively). Interestingly, only the former is recognized by the next enzyme of the phenylpropanoid pathway (i.e., CINNAMATE-4-HYDROXYLASE) and hence acts as a pathway intermediate (Pfändler et al., 1977). *c*-CA is a UV-mediated conversion product of *t*-CA and is not further channeled in the pathway (Wong et al., 2005; Yang et al., 1999; Yin et al., 2003). The first report on the bioactivity of CA dates back to 1935, when *c*-CA (at that time termed allocinnamic acid) was found to have a positive effect in different auxin bioassays, whereas this was not the case for *t*-CA (Haagen-Smit & Went, 1935; Hitchcock, 1935). Since then, the difference in the biological activity of both isomers was confirmed in a range of experiments performed on different plant species (Veldstra, 1944, 1953). The link of *c*-CA with auxin homeostasis was later established by showing that *c*-CA acts as an inhibitor of auxin transport (Steenackers et al., 2017).

Although the activity of *c*-CA is unambiguously proven (Steenackers et al., 2019), the activity of *t*-CA is still a matter of debate. Despite the many reports referring to the absence of activity, several studies demonstrated an effect on cell elongation. For example, Morris and Arthur (1984) reported a *t*-CA-mediated stimulation of elongation in internodal segments of *Phaseolus vulgaris* and claimed that *t*-CA acts as a competitive inhibitor of auxin. Others stated an antagonizing effect of *t*-CA on the stimulatory action of auxin on the elongation of pea stem sections (Van Overbeek et al., 1951). The anti-auxin activity of *t*-CA was later confirmed by others (Audus, 1972; Letham et al., 1978). More recently, it was demonstrated that *t*-CA feeding of *Arabidopsis thaliana* leads to auxin-dependent leaf expansion and petiole elongation (Kurepa et al., 2018). In contrast to the observed positive effect of *t*-CA on cell elongation, an inhibitory effect on elongation has been reported on the roots of lettuce (Fujita & Kubo, 2003) and Arabidopsis seedlings (Abenavoli et al., 2008) and on the 2,4-D-triggered growth of pea internodes (Masuda & Tanimoto, 1967). Although the observed difference in activity could be a dose–response effect, whereby the compound is getting toxic at higher concentrations, others showed that the inhibitory effect was independent of the *t*-CA concentration used (Li et al., 1993). Using conditions excluding *trans-cis* isomerization, the growth-promoting effect of *t*-CA on Arabidopsis was later demonstrated as a pure *c*-CA effect, questioning the claimed activity of *t*-CA in previous studies where isomerization could not be excluded (Vanholme et al., 2019).

In this paper, we aim to elucidate the potential activity of *t*-CA and *c*-CA on cell elongation and used a submerged rice (*O. sativa* L.) coleoptile assay for this. Because the assay is performed in the dark, photo-isomerization between *t*-CA and *c*-CA can be excluded. Next to answering the question of whether or not *t*-CA and *c*-CA indeed cause growth effects in rice coleoptiles, we also used the assay to unravel the molecular mechanisms at play. We combined transcriptomics and (untargeted) metabolomics with activity assays and genetic and pharmacological experiments and focused notably on the interplay between CA isomers and auxin-mediated cell growth to explain the underlying mechanistic processes.

2 | MATERIALS AND METHODS

2.1 | Plant materials

Experiments were carried out with *O. sativa* (L.) cv (New) Dongjin unless stated differently. Seeds of the DR5-VENUS line, in which a synthetic auxin-responsive promoter (DR5rev) was used to drive expression of the *YELLOW FLUORESCENT PROTEIN* (*YFP*), were kindly provided by prof. Zhang of the Shanghai Jiaotong University (Yang et al., 2017). Seeds of the Nipponbare *WRKY45* RNAi lines were kindly provided by prof. Takatsuji (National Institute of Agrobiological Sciences, Ibaraki, Japan) (Shimono et al., 2007).

2.2 | Rice coleoptile elongation assay: A tool to assess cell elongation *in planta*

2.2.1 | Seed sterilization

Rice seeds were disinfected as described (Narsai et al., 2015). In short, the seeds were dehusked and surface-sterilized with 70% (v/v) ethanol for 1 min, followed by a 1-min washing step in sterile distilled H_2O. Then, seeds were subjected to 2.5% (v/v) bleach for 10 min, three times to sterile distilled H_2O for 1 min, once to 0.1% (w/v) mercuric chloride for 3.5 min, and five times to sterile distilled H_2O for 1 min. During the incubation steps, seeds were continuously shaken.

2.2.2 | Pre-germination and seedling growth

The sterilized seeds were pre-germinated in Petri dishes (90 × 20 mm; SPL Life Sciences) containing a sterile filter paper (90-mm diameter; Whatman) by complete submergence in 2.0 mM

$CaSO_4$ (Köhl, 2015; Magneschi et al., 2009). The Petri dishes were closed with 3 M Surgical Tape (Micropore) and kept in continuous darkness at a 12-h/12-h day/night cycle and 28°C/26°C temperatures. After 2 days, seedlings with a similar coleoptile development were selected and transferred under sterile conditions in the dark under green safety light to 50-ml conical centrifuge tubes (SPL Life Sciences). These tubes contained 50 ml 2.0-mM $CaSO_4$, either supplemented with the CA isomers or not (see the next section). Each 50-ml tube contained five seedlings, and for each treatment, three tubes were filled. The tubes were closed, placed in a 50-ml centrifuge tube rack, wrapped in four layers of tin foil, and placed back in the growth chamber at a 12-h/12-h day/night cycle and 28°C/26°C temperatures.

2.2.3 | CA treatment and coleoptile length measurement

For long treatments, *t*-CA or *c*-CA was added immediately after the transfer of the 2-day-old seedlings to 50-ml tubes, and analysis was done 1–8 days after transfer (DAT). For short treatments, the isomers were added at 3 DAT, and analysis was done 1, 3, 6, 12, or 24 h after the start of the treatment. After several hours/days of growth in 50-ml tubes, coleoptiles were dissected from the seedlings and cleared using a protocol adjusted from Nelissen et al. (2013). Coleoptiles were treated with ethanol:acetic acid (3:1) for 2 days before being positioned on a square dish (245 × 245 mm; SPL Life Sciences) filled with 0.66% (w/v) Plant Tissue Culture Agar (Neogen) and scanned (in color at 600 dpi). The obtained coleoptile images were analyzed using Plength, an in-house developed program for the automated analysis of rice seedling lengths (Vlaminck et al., 2020). For contrast purposes and as a reference, a black background with a 2-cm scale bar in one of the lower corners was placed behind the plate with coleoptiles before scans were made.

2.2.4 | Cellular analysis

To measure cell lengths and widths in the epidermal layers of the basal and uppermost zones of the coleoptiles, the method described in Pan et al. (2000) was adapted. Briefly, cleared coleoptiles were transferred to 50% glycerol and put on a slide for optimal image acquisition under the light microscope. For the tip and base measurements (first 5 mm), 10 cells in one or several cell files were used to measure cell length and width. Also, one complete central cell file was followed from tip to base.

2.3 | Microscopy

Epidermal cell layers for cellular analysis were imaged using a BXS3T-32F/PH/DIC Leica microscope, DP27 camera, and CellSens Standard software or a Zeiss Axio Imager. DR5-VENUS seedlings were analyzed using an SZX10 Olympus microscope, DigiRetina camera, and TcCapture software with a GFP filter.

2.4 | Hormonal measurements

For each treated seedling in five repeats, the coleoptile was removed, snap frozen, ground with mortar and pestle, and stored at −80°C. This was done in the dark under green safety light to avoid photoisomerization of compounds. One hundred milligrams of each sample were used for further manipulations as described by Haeck et al. (2018). Briefly, a cold-modified Bieleski solvent was used for extraction, followed by centrifugal filtration and cleanup. Hormones were separated and measured by an ultrahigh performance liquid chromatography (UHPLC) system coupled to a Q-Exactive™ quadrupole Orbitrap mass spectrometer, operating at a mass-resolving power of 70,000 full width at half maximum.

2.5 | Metabolome study

2.5.1 | Sample preparation

Coleoptiles were prepared as described in the previous section (section 2.2). Each sample consisted of five coleoptiles; in total, eight samples were harvested per treatment. Samples were transferred to a 2-ml Eppendorf tube containing two 4-mm stainless-steel balls, snap frozen and homogenized using a bead beater (Retsch MM301) for 40 s at 20 Hz. Samples were extracted with 1 ml methanol for 20 min followed by centrifugation at 14,000 rpm for 5 min at room temperature. The methanol was transferred to a new 2-ml Eppendorf tube and both the pellet and the methanol fraction were completely dried using a CentriVap Benchtop Vacuum Concentrator (Labconco). The pellet was weighted and used for LC–MS data normalization; the dried methanol fraction was reconstituted in 100 µl milliQ, vortexed, and centrifuged at 14,000 rpm for 5 min at room temperature. Finally, 80 µl was filtered and transferred into a 96-well plate for LC–MS analysis. All steps were performed in the dark as much as possible to avoid photoconversion.

2.5.2 | LC–MS

LC–MS analysis was performed on an ACQUITY UPLC I-Class system (Waters) consisting of a binary pump, a vacuum degasser, an autosampler, and a column oven. Chromatographic separation was carried out on an ACQUITY UPLC BEH C18 (150 × 2.1-mm, 1.7-µm) column from Waters, and the temperature was maintained at 40°C. A gradient of two buffers, buffer A (99:1:.1 water:acetonitrile:formic acid, pH 3) and buffer B (99:1:.1 acetonitrile:water:formic acid, pH 3), was used as follows: buffer A decreased from 99% to 50% from 0 to 30 min, and buffer B decreased from 99% to 0% from 30 to 40 min. The flow rate was set to 0.35 ml min^{-1}, and the injection volume was 10 µl.

The UHPLC system was coupled to a Vion IMS QTOF hybrid mass spectrometer (Waters). The LockSpray ion source was operated in negative electrospray ionization mode under the following specific conditions: capillary voltage, 2.5 kV; reference capillary voltage, 2.5 kV; cone voltage, 30 V; source offset, 50 V; source temperature, 120°C; desolvation gas temperature, 550°C; desolvation gas flow, 800 L h^{-1}; and cone gas flow, 50 L h^{-1}. The collision energy for MSe was set at 6 eV (low energy) and ramped from 20 to 70 eV (high energy); the intelligent data capture intensity threshold was set at 5. For DDA-MSMS, the low mass ramp was ramped between 15 and 30 eV, and the high mass ramp was ramped between 30 and 70 eV. Nitrogen (greater than 99.5%) was employed as desolvation and cone gas. Leucin–enkephalin (250 pg μl^{-1} solubilized in water: acetonitrile 1:1 [v/v], with 0.1% formic acid) was used for the lock mass calibration, with scanning every 2 min at a scan time of 0.1 s. Profile data were recorded through a UNIFI Scientific Information System (Waters). Data processing was performed with Progenesis QI software version 2.4 (Waters). Data analysis was done using MetaboAnalyst 4.0 (www.metaboanalyst.ca).

2.6 | Measurement of ATP hydrolytic activity of plasma membrane H^+-ATPase

To be able to measure the ATP hydrolytic activity of plasma membrane H^+-ATPase in rice coleoptiles, we based ourselves on the protocol of Okumura and Kinoshita that uses *A. thaliana* leaves (Kinoshita et al., 1995; Okumura & Kinoshita, 2016). We used an adaptation of the procedure to prepare microsomal membranes from rice coleoptiles. Fifty coleoptiles per sample were homogenized with mortar and pestle in a 6-ml ice-cold homogenization buffer and were kept on ice. The homogenate was centrifuged at 13,000 g for 10 min at 4°C using a Thermo Scientific™ FiberliteTM F21-8x50y rotor. Next, the supernatant was transferred into Polyallomer Centrifuge Tubes (14 × 89 mm; Beckman) and ultracentrifuged (Beckman L8–70, SW41 rotor) at 100,000 g for 1 h at 4°C before the obtained pellet was resuspended in a 100-µl ice-cold homogenization buffer, and the protein concentration was quantified and adjusted.

Next, we measured the vanadate-sensitive ATP hydrolytic activity, as described by Okumura and Kinoshita (2016). Plant plasma membrane H^+-ATPase couples ATP hydrolysis to H^+ extrusion and thereby generates an electrochemical gradient across the plasma membrane. Plant cells contain many ATP hydrolytic enzymes, which makes it sometimes difficult to determine the ATP hydrolytic activity of the plasma membrane H^+-ATPase, a P-type ATPase. KNO_3 was used as an inhibitor of V-type ATPases, ammonium molybdate as an inhibitor of acid phosphatases, oligomycin as an inhibitor of F-type ATPases, and NaF as an inhibitor of phosphatases. Orthovanadate inhibits the P-type ATPases and thus can be used to measure the activity of the plasma membrane H^+-ATPase by assessing the vanadate-sensitive Pi release from ATP hydrolysis. The released Pi reacts with molybdate to form a blue complex, which can then be quantified by measuring the absorption at 750 nm.

2.7 | Analysis of cell wall esterified hydroxycinnamic acid

2.7.1 | Sample preparation

For the analysis of esterified hydroxycinnamic acids in the cell wall, adjustments were made to the protocol described by Bartley et al. (2013). Seedlings were placed for 24 h in a 2.0-mM $CaSO_4$ solution with 10-µM *c*-CA, 10-µM [$^{12}C_6$]-/[$^{13}C_6$]-*t*-CA, or DMSO (control). *c*-CA and [$^{12}C_6$]-*t*-CA were purchased from Chem Space and Sigma-Aldrich, respectively. RING-$^{13}C_6$-*t*-CA was purchased from Cambridge Isotope Laboratories (Andover, MA). Next, cell wall material of 15 pooled coleoptiles was prepared. Elongating coleoptiles were harvested and dried at 60°C for 24 h in the dark. After drying, the tissue was ground for 60 s at 20 Hz with a tissue homogenizer in 2-ml safe-lock Eppendorf tubes with two 4-mm stainless-steel balls. The tissue was treated with 1.5 ml 95% ethanol at 99°C for 30 min. A weight was put on these samples to avoid ethanol evaporation. Afterward, the supernatant was removed by centrifugation (10,000 g; 10 min), and the residue was subsequently washed three times with 1 ml 70% ethanol and each time centrifuged for 1 min at 10,000 g. Subsequently, the samples were dried for 2 h at approximately 35°C under vacuum using a CentriVap Benchtop Vacuum Concentrator (Labconco). To release esterified hydroxycinnamic acids from the cell wall samples, the dried powder was saponified with 500 µl of 2-M NaOH for 24 h at 25°C with mixing at 300 rpm. After saponification, the supernatant was acidified to pH < 2 with 100 µl 37% HCl, vortexed, and extracted three times with 300 µl ethylacetate. The extracts were combined and evaporated to dryness for 1.5 h using a CentriVap Benchtop Vacuum Concentrator (Labconco) at 32°C. Next, samples were resuspended in 100 µl 4% acetonitrile.

2.7.2 | LC–MS profiling

For LC–MS analysis, 10 µl was injected for each sample. Instrument settings were as described above, except that the mass range was set at 50–1000 Da, HDMSe was enabled, and capillary voltage was set at 3 kV.

2.7.3 | LC–MS data processing

Chromatograms were processed with Progenesis QI software version 2.4 (Waters Corporation). The raw data were imported using a filter strength of 1. A pooled sample was chosen as a reference for alignment purposes. Peak picking was based on the aggregate of all runs with a sensitivity set at maximum sensitivity. In total, 11,924 *m/z* features (compound ions) were integrated and aligned across all chromatograms. Data normalization was done on the dry weight of the samples. Four hundred one MS/MS spectra were recorded and exported to an msp file.

The untargeted selection of all ^{13}C-labeled *m/z* features was done using the Generate_DoubletFile (rt_diff = 3, error = 0.002, cutoff = 100, massdiff = "C6," mass = 6.02013) function of the *in-house*-developed RDynSIL package and yielded 279 labeled *m/z* features (corresponding with 166 compounds), for which 108 MS/MS spectra were recorded. Seventy-one *m/z* features had a feature abundance that was significantly higher ($p < 0.05$) in the seedlings treated with $[^{12}C_6]$-/$[^{13}C_6]$-*t*-CA as compared to the seedlings treated with *c*-CA and compared the control samples. For 28 out of the 71 *m/z* features, an MS/MS spectrum was recorded. All statistics were performed in R version 4.2 on arcsinh-transformed ion intensities. One-way analysis of variance (ANOVA) followed by Bonferroni post hoc tests ($p < 0.05$) were performed with the lm function and the pairwise.t.test function, respectively.

2.8 | Differential expression analysis: RT-qPCR and RNA-sequencing (RNA-seq)

2.8.1 | Sample preparation

Coleoptiles were pre-germinated for 2 days as described above, transferred to 50-ml tubes, and only 3 days after this transfer, during the exponential growth of the coleoptile, 10-μM *c*-CA or 50-μM *t*-CA was added. Next, coleoptiles were harvested at 1, 12, and 24 h after the start of the treatment. In the dark, under green safety light, the coleoptiles were dissected, snap frozen in liquid nitrogen, ground in a mortar, and stored at −80°C. Each sample consisted of 20 pooled coleoptiles.

2.8.2 | RNA extraction and cDNA synthesis

RNA was extracted with the Zymo Research Direct-zol™ RNA MiniPrep Plus kit using a slightly adapted extraction protocol. Frozen tissue samples were lysed by adding 1 ml TRIzol reagent (Invitrogen). Next, samples were vortexed and left at room temperature for 5 min before vortexing a second time. Debris was removed by centrifuging the samples and transferring the supernatant to an RNase-free tube. The next steps were performed as described in the kit's protocol, with the exception of the DNase I treatment, which was performed by adding a mixture of 5-μl RQ1 RNase-free DNase (Promega) and 75-μl RQ1 DNase 10X Reaction Buffer (Promega) directly to the column matrix of each sample before incubating them during 30 min at room temperature. Promega products were preferred above the alternative supplied with the kit as they gave superior results. Moreover, during the last washing step, samples were centrifuged for 2.5 min instead of 1 min to ensure the complete removal of Wash Buffer. Finally, mRNA was eluted by adding 50 μl of DNase/RNase-free water directly to the columns. RNA concentration and purity of each sample were assessed via spectrophotometry (Nanodrop® ND-1000). Finally, 1 μg RNA was used to synthesize cDNA via the iScript™ cDNA Synthesis Kit, following the manufacturer's instructions.

2.8.3 | RT-qPCR

All RT-qPCR experiments were performed in three to four biological repeats and three technical repeats using 384-multiwell plates and detection by SYBR® Green. Reaction mixes were composed with a final volume of 5 μl and a 10% cDNA fraction using the SYBR® Green Master Mix (PerkinElmer). The mix is composed of PCR buffer with SybRGreen, $MgCl_2$, dNTPs, DNA polymerase, and the designed primers. All qPCR reactions were executed with a Roche Lightcycler® 480 system (Roche Diagnostics) using the following settings: one pre-incubation step at 95°C for 8 min, followed by 40 cycles of amplification at 95°C for 15 s, 60°C for 10 s, and 72°C for 10 s. After the final cycle, a melting curve was recorded: 95°C for 5 s followed by heating from 95°C to 97°C for 1 min and cooling down to 40°C for 10 min. The Lightcycler® 480 software was used to determine C_t-values and efficiencies, and these were analyzed using the 2-ΔΔCt method (Livak & Schmittgen, 2001). The obtained expression data were normalized to the expression levels of the housekeeping genes *UBQ5* encoding UBIQUITIN 5 and *G3PDH* encoding GLUCOSE-3-PHOSPHATE DEHYDROGENASE (Hsu & Tung, 2017; Jain et al., 2006; Kumar et al., 2018). Primer sequences were taken from their respective reference paper if possible. Otherwise, they were designed using the Roche Universal ProbeLibrary Assay Design Center (https://lifescience.roche.com/). All primers were diluted with nuclease-free water to a final concentration of 10 μM. Primer sequences are summarized in Table S1.

2.8.4 | cDNA library preparation for RNA-seq

The sequencing was performed at the Nucleomics Core Facility of the VIB (Leuven, Belgium; www.nucleomics.be). RNA quality and purity (A260/A280 and A260/A230 ratios >1.8) were rechecked using a Bioanalyzer Nano (Agilent Technologies), and all samples had a quality documented by RIN values >8. Library preparation, pooling, and sequencing were performed with the Illumina HiSeq 4,000, using the SBS 50 Kit (2.25 nM + 1% PhiX v3), single end (76-8-8-0).

2.8.5 | Data processing

Demultiplexing and subsequent data analysis steps were performed in Galaxy (https://usegalaxy.org/). The pipeline consisted of quality control with FASTQC, filtering of the adaptor, and other overrepresented sequencing with Trimmomatic (Bolger et al., 2014). The remaining reads were mapped to the *O. sativa* (L.) ssp. japonica reference genome, using SALMON. Venny 2.1 (Oliveros, 2015) and MAPMAN (Thimm et al., 2004) were used for the representation of the results.

Statistical analysis was performed with the R software package edgeR (R core team, 2014; Robinson et al., 2010) (R version 3.6.2). Only genes with an expression value higher than 0.25 cpm (corresponding to five read counts) in at least three samples were retained for the analysis. TMM normalization (Robinson & Oshlack, 2010) was

applied using the calcNormFactors function. Variability in the dataset was assessed with MDSplot. The treatment and time factors were collapsed into one factor. Trended negative binomial dispersion parameters were estimated based on an additive no intercept model with the collapsed factor and a batch effect using the estimateDisp function and down-weighting outlying genes. A quasi-likelihood negative binomial regression model (Lund et al., 2012) was then used to model the overdispersed counts for each gene separately as implemented in the function glmQLFit using the above-described model. The research question was to find genes that act differently over time between the treatments. Contrasts were estimated using empirical Bayes quasi-likelihood F-tests. In addition, treatment differences were compared at the three time points; *p*-values were corrected using the FDR method described by Benjamini and Hochberg (1995). All edgeR functions were applied with default values. A gene was called differentially expressed when the FDR value was <0.05.

2.8.6 | Data representation

A weighted correlation network analysis was performed using the WGCNA package (version 1.71) in R (version 4.2.1) (Langfelder & Horvath, 2008). The rice gene IDs were converted from the MSU to RAP type using the riceidconverter package (version 1.1.1) prior to gene ontology (GO) enrichment analysis (Li, 2020). The rice gene GO annotations for this analysis were extracted from the RAP-DB and OryzaBase public rice gene annotation databases following the protocol of Li (2022). The *enricher* function of the clusterProfiler package (version 4.4.4) was used for GO enrichment analysis (Wu et al., 2021).

Monocots PLAZA 4.0 was used to link the obtained gene identifiers with gene descriptions, biological processes, and molecular functions and to perform a GO enrichment analysis (Van Bel et al., 2018). After clustering the differentially expressed genes based on their ontology, we visualized the biological processes and molecular function of those using Revigo (Supek et al., 2011). We also used Venny 2.1 (Oliveros, 2015) and MAPMAN (Thimm et al., 2004) for the representation of the results. Note that the processed RNA-seq results solely contain *t*-CA and *c*-CA treatment expression levels, which in fact represent the expression of *t*-CA and *c*-CA minus mock expression.

2.9 | Statistical analysis

For the experiments where it is not specified above, the statistical package "R version 3.6.0" (www.r-project.org/) was utilized. To address the statistical difference between two or more experimental groups, an ANOVA (linear mixed-effects model) was used. All pairwise comparison tests were performed with Tukey's test. The statistical assumptions of normality (via histogram) and homogeneity of variances (by the analysis of residuals, QQ-plot) were tested and were needed, and log-transformations were applied, when the data did not comply. For the analysis of the relative gene expression obtained via RT-qPCR, hormonal measurements, and H^+-ATPase activity, a Kruskal–Wallis rank-sum test was performed, followed by a Bonferroni correction (Hollander & Wolfe, 1973).

3 | RESULTS

3.1 | *t*-CA and *c*-CA treatments have opposite effects on rice coleoptile cell elongation

We examined the effect of *c*-CA and *t*-CA on coleoptile elongation by submerging 2-day-old pre-germinated rice seeds in a *c*-CA or *t*-CA solution. At 5 DAT, *t*-CA treatment significantly decreased the total coleoptile length, in comparison to the mock-treated seedlings, whereas *c*-CA led to a significant increase in coleoptile length, both in a concentration-dependent manner (Figure 1a-b). Further experiments were done with 50-μM *t*-CA and 10-μM *c*-CA, as these were the lowest concentrations that resulted in clear and significant phenotypes. In a subsequent temporal analysis from 1 to 8 DAT, it was shown that compared with the mock, continuous *t*-CA treatment significantly impeded growth already from 2 DAT onward, whereas continuous *c*-CA treatment induced a significantly faster growth starting from 4 DAT (Figure 1c). To further pinpoint the onset of the growth effects, we analyzed the effect of 1-, 3-, 6-, 12-, and 24-h CA treatment of coleoptiles that were already growing (and elongating) in a mock medium for 3 days (3 DAT). Only by the 24-h treatment, significant differences in coleoptile lengths induced by both *t*-CA and *c*-CA treatments could be observed (Figure 1d).

We also checked the effect of both CA isomers on the cell dimensions in the epidermal layer of the coleoptile. A steep increase in length of the first 5 to 10 cells in the tip of *c*-CA-treated coleoptiles could be demonstrated (Figure 1e), whereas *t*-CA treatment resulted in shorter cells as compared with the mock-treated coleoptiles (Figure S1A). Moreover, although *c*-CA treatment had no effect on the base of the coleoptile, *t*-CA treatment clearly inhibited base cell elongation, starting already from the third mm (Figure S1C). In contrast to cell length, cell width was not affected, in tip or base, by any treatment (Figure 1f, Figure S1B and D). We also noted a difference in the total number of cells upon the different treatments: *c*-CA-treated coleoptiles had on average a higher cell number, and *t*-CA-treated coleoptiles had a lower cell number, compared with the mock (Figure 1e). This indicates that not only cell elongation is affected by CA, but, to a minor extent, also cell division plays a role in coleoptile elongation length in our experimental setup.

To determine whether the effects are caused by *t*-CA and *c*-CA specifically, we examined possible phenotypes caused by a number of CA-dimers and CA-conversion products. None of the tested dimers (i.e., alpha-truxillic acid and beta-truxinic acid, often converted from *c*/*t*-CA [Bernstein & Quimby, 1943]) affected coleoptile length (Figure S2A-B). In addition, none of the tested downstream intermediates of the phenylpropanoid pathway (i.e., *p*-coumaric acid [*trans* and UV-treated, i.e., to obtain a *trans-cis* mixture], *trans*-ferulic acid [FA], and the monolignols *p*-coumaryl alcohol, coniferyl alcohol, and sinapyl

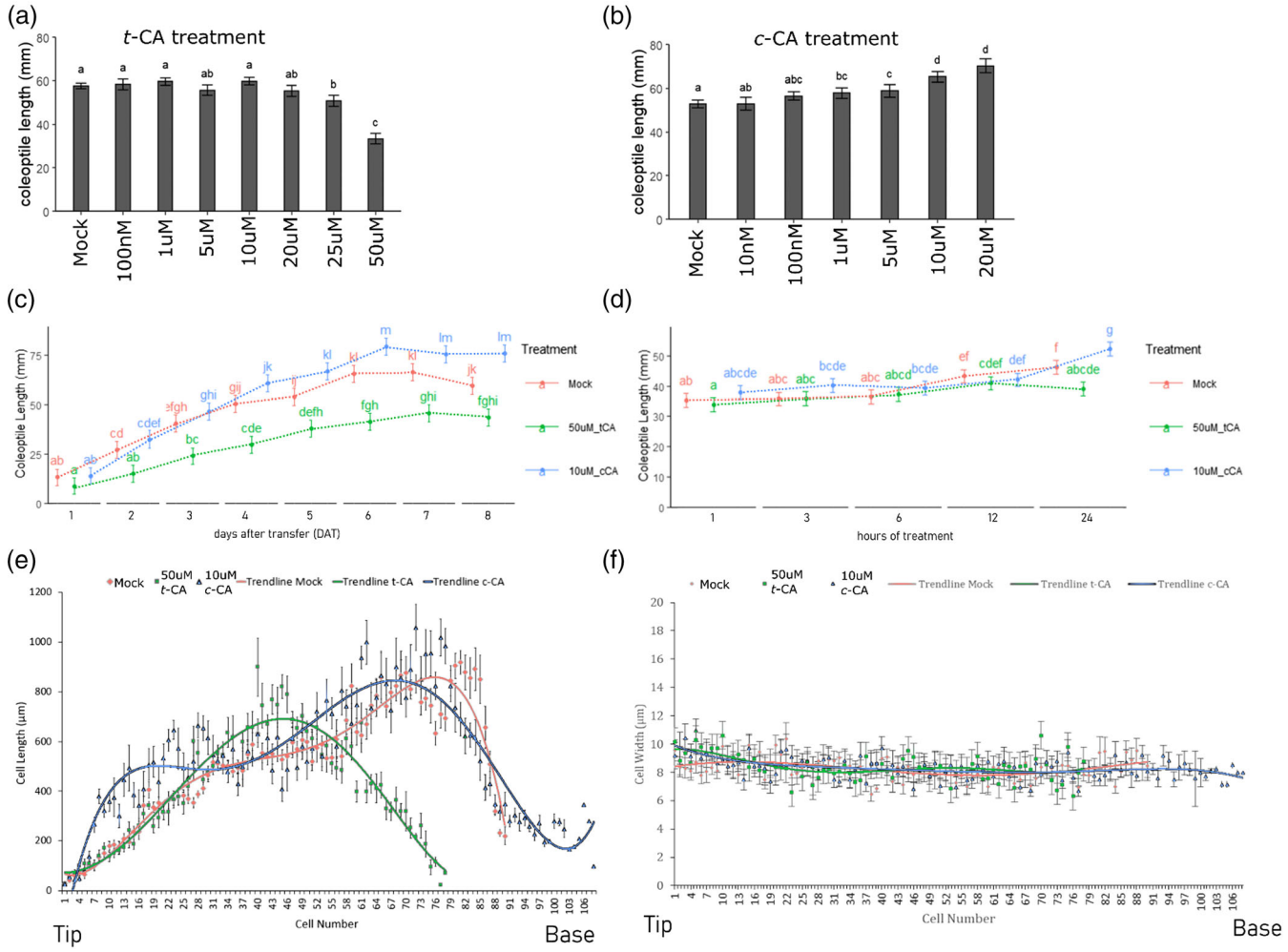

FIGURE 1 Phenotypic effects of *t*-CA and *c*-CA treatment on coleoptile and cell lengths. (a) Effect of 100-nM, 1-µM, 5-µM, 10-µM, 20-µM, 25-µM, and 50-µM *t*-CA treatment on rice coleoptile length at 5 DAT ($n \geq 45$). (b) Effect of 10-nM, 100-nM, 1-µM, 5-µM, 10-µM, and 20-µM *c*-CA treatment on rice coleoptile lengths at 5 DAT ($n \geq 45$). (c) Average coleoptile length over time in DAT for DMSO (mock), 50-µM *t*-CA, or 10-µM *c*-CA-treated coleoptiles ($n \geq 41$). (d) Average coleoptile length over time in hours after the start of treatment at 3 DAT for DMSO (mock), 50-µM *t*-CA, or 10-µM *c*-CA-treated coleoptiles ($n \geq 57$). (e–f) effect of 50-µM *t*-CA and 10-µM *c*-CA treatment on cell length (e) and cell width (f) over the whole length of coleoptiles ($n = 12$, except for the highest cell numbers, which consist of one to three data points due to the differences in coleoptile length).

alcohol) affected coleoptile length (Figure S2G-L). A treatment with piperonylic acid (PA), leading to *in planta* *t*-CA accumulation by blocking CINNAMATE 4-HYDROXYLASE (C4H) (El Houari et al., 2021; Schalk et al., 1998), decreased coleoptile elongation (Figure S2C). The inhibitory effect obtained by PA could not be restored by a co-treatment with *p*-coumaric acid to rescue the downstream pathway (Figure S2D), whereas a co-treatment with *t*-CA resulted in an additive inhibitory effect (Figure S2E). In contrast, a co-treatment of PA with *c*-CA resulted in a rescue of the PA phenotype but not to the extent of the *c*-CA phenotype alone (Figure S2F).

Altogether, these data showed that *t*-CA inhibits and *c*-CA enhances coleoptile cell elongation, in specific zones of the coleoptile, and this is in a concentration-dependent manner. The observed effects on cell elongation are most likely direct effects of *t*-CA and *c*-CA and not triggered by a more downstream-derived phenylpropanoid. In addition, the observation that *c*-CA rescued the PA phenotype suggests both CA isomers act via independent mechanisms.

To obtain insight into the mechanistic changes and signaling processes behind the noted opposite elongation effects, we looked into transcriptome changes upon *t*-CA and *c*-CA treatment. Initial exploration of the RNA sequencing experiments through weighted correlation network analysis (cf. Materials and Methods) revealed a negative correlation between coleoptile length and genes involved in biological processes such as stress and defense responses (among others, response to deep water), hormone pathways (i.e., jasmonic acid and salicylic acid [SA]), flavonoid biosynthesis, protein metabolism, and photosynthesis. Interestingly, in terms of molecular function, UDP glycosyltransferase activity was negatively correlated with elongation: possibly hinting at cell wall polysaccharide synthesis adding to cell

wall rigidity. Positive correlation on the other hand was found with transport processes, as well as processes such as cell division, cellular metabolism, protein turnover, and DNA/RNA metabolism. Gibberellin and brassinosteroid responses, both well known to induce elongation, were also noted. Furthermore, GO categories in hydrolase and cellulase activity were enriched, linking the data with the loosening of the cell wall, which subsequently allows for elongation (data not shown).

In the below sections, we analyzed the transcriptome changes in more detail and coupled them to metabolome changes in order to get insight into how *c*-CA and *t*-CA affect elongation processes in submerged rice coleoptiles.

3.2 | *t*-CA restricts cell elongation by increasing feruloylation and/or channeling toward SA

A total of 368 differentially expressed genes were significantly downregulated upon *t*-CA treatment at all three time points (1, 12, and 24 h, Figure S3). A GO enrichment analysis ($p < 0.05$) via monocot PLAZA 4.0 (Figure S4) showed clear involvement of cell wall modifications (including regulation of pectin biosynthesis, microtubule polymerization/bundle formation, and oligosaccharide metabolism).

Furthermore, the upregulation of genes in the phenylpropanoid pathway upon *t*-CA treatment was apparent upon MAPMAN analysis, whereas this was not the case upon *c*-CA treatment (Figure S5A-B), which is in line with the fact that only *t*-CA is channeled into the phenylpropanoid pathway. The key gene *C4H* (LOC_Os05g25640), for instance, was significantly higher expressed upon *t*-CA treatment (LogFC of 2.16, 1.33, and 1.88 for 1, 12, and 24 h of *t*-CA treatment, respectively).

The transcriptome data also indicated that putative arabinoxylan feruloyl transferase (AFT)-encoding genes (i.e., Os01g09010 and Os05g0564) were significantly more highly expressed in *t*-CA-treated coleoptiles. FA, when incorporated in the primary cell wall of coleoptiles, serves to cross-link different arabinoxylan cell wall polysaccharides via diferulate and oligoferulate bridges. This feruloylation makes the cell wall more rigid and hence restricts elongation (Buanafina, 2009; Mnich et al., 2020). In a subsequent RT-qPCR experiment, we confirmed the differential expression of putative *AFT* genes in a time-dependent manner (Figure 2a-e). Metabolomics data confirmed these observations at the metabolite level: *t*-FA content (next to several FA dimers, as well as *p*-coumaric acid and ethyl-*p*-coumarate) was indeed significantly higher upon *t*-CA treatment, at both 3 and 5 DAT as compared with mock and *c*-CA treatment (Figure 2f-h). Additionally, we measured hydroxycinnamic acids in the cell wall fraction after the treatment of coleoptiles with ^{13}C-labeled *t*-CA. Labeled FA, derivatives, and oligomers were detected in ^{13}C *t*-CA-treated samples, showing that *t*-CA is at least partly converted into FA (Figure 2i-n).

Interestingly, the metabolomics analysis also revealed that benzoic acid and its derivatives, including SA-derived compounds, accumulated in *t*-CA-treated coleoptiles (Figure 3a-c). This is noteworthy, since *t*-CA can easily be converted into SA via benzoic acid (Lefevere et al., 2020; Shah, 2003) and SA has recently been linked with plant growth attenuation (Tan et al., 2020). *ABNORMAL INFLORESCENCE MERISTEM1* (*AIM1*, Os02g17390), encoding a regulator of the latter process (Lefevere et al., 2020), is upregulated upon *t*-CA treatment (LogFC of 2.16, 1.77, and 1.41 for 1, 12, and 24 h of *t*-CA treatment, respectively). Remarkably, when we specifically measured the levels of free SA after a short 50-μM *t*-CA treatment of 1, 12, and 24 h, and at 3 and 5 DAT, only a significant decrease in SA levels could be noted at 3 DAT (Figure 3e-i). The absence of an effect at 5 DAT possibly indicates that homeostasis is at play to maintain constant free SA levels. We evaluated these findings by adding SA in the coleoptile elongation assay and found an inhibitory effect in a concentration-dependent manner similar to *t*-CA treatment (Figure 3d). Additionally, *WRKY45* RNAi lines that cannot activate a SA response showed to be nonresponsive to *t*-CA treatment (Figure 3j-l), indicating that *t*-CA could act through SA metabolism and/or SA signaling.

Taken together, these data point out that *t*-CA treatment stimulates feruloylation as well as SA metabolism, both of which can make the cell wall more rigid (Rivas-San Vicente & Plasencia, 2011) and hence could explain the observed restriction of cell elongation.

3.3 | *c*-CA effects on cell elongation rely on apoplast acidification

Upon *c*-CA treatment, 21 genes were constitutively upregulated from 1 h of treatment onward (Figure S3A, Table S5). Several of these genes are related to ATPase activity, transmembrane transport, and notably, auxin involvement, which are all linked to monopolar growth. This was even further exacerbated by the lists of upregulated genes at the specific time points (1, 12, and 24 h) after treatment (Tables S2–S4).

ATPase activity is crucial for the acidification of the apoplast, which in its turn is necessary for auxin-induced coleoptile elongation (Du et al., 2020; Narsai et al., 2015). To further study the involvement of ATPases by *c*-CA treatment, we added N,N′-dicyclohexylcarbodiimide (DCC(D)), an inhibitor of the proton-conducting activity of H^+-ATPases (Nelson & Harvey, 1999), to the CA treatments. DCC(D) treatment alone led to shorter coleoptiles, since it inhibits acidification of the apoplast (Figure 4a). The addition of indole-3-acetic acid (IAA) to DCC(D)-treated coleoptiles could not restore the phenotype (Figure 4a). Importantly, *c*-CA-induced elongation was impaired upon DCC(D) addition. Moreover, the ATP hydrolytic activity of plasma membrane H^+-ATPases was found to be significantly higher in *c*-CA-treated coleoptiles as compared with DMSO- and/or *t*-CA-treated coleoptiles during coleoptile growth (at 3 DAT). Moreover, it was quantitatively comparable to IAA treatment (Figure 4b). This indicates that *c*-CA leads to a higher proton conducting activity in the plasma membrane, which is necessary for the acidification of the apoplast. This in turn could lead to the loosening of the cell wall, a necessity for elongation growth (Arsuffi & Braybrook, 2017).

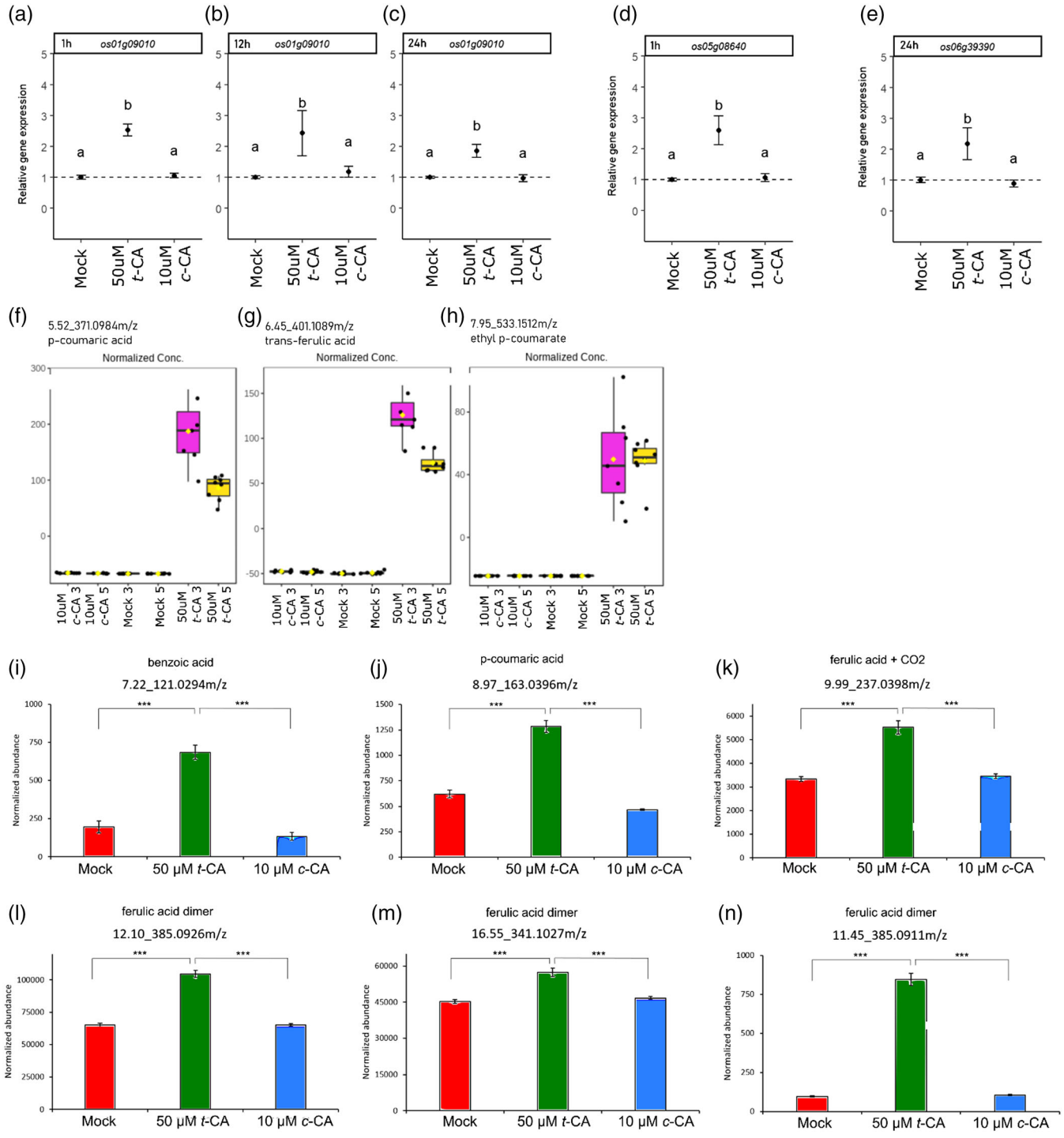

FIGURE 2 Stimulation of feruloylation in the cell wall by *t*-CA treatment. (a–e) relative gene expression of two putative arabinoxylan feruloyl transferase genes that are more highly expressed in 50-μM *t*-CA-treated coleoptiles compared to 10-μM *c*-CA- and DMSO (mock)-treated coleoptiles at different time points. Different letters indicate statistically significant differences at $p < 0.05$ ($n \geq 3$). (f–h) abundance normalized for dry weight of *p*-coumaric acid (f), *trans*-FA (g), and ethyl *p*-coumarate (h) found in an untargeted metabolomics experiment with coleoptiles treated with 50-μM *t*-CA or 10-μM *c*-CA and analyzed at 3 DAT (3) or 5 DAT (5). (i–n) compound abundance corrected for dry weight of compounds that are significantly more abundant in the cell wall of rice coleoptiles treated with 50-μM *t*-CA as compared to DMSO- and 10-μM *c*-CA-treated samples (*** < 0.001, $n \geq 8$).

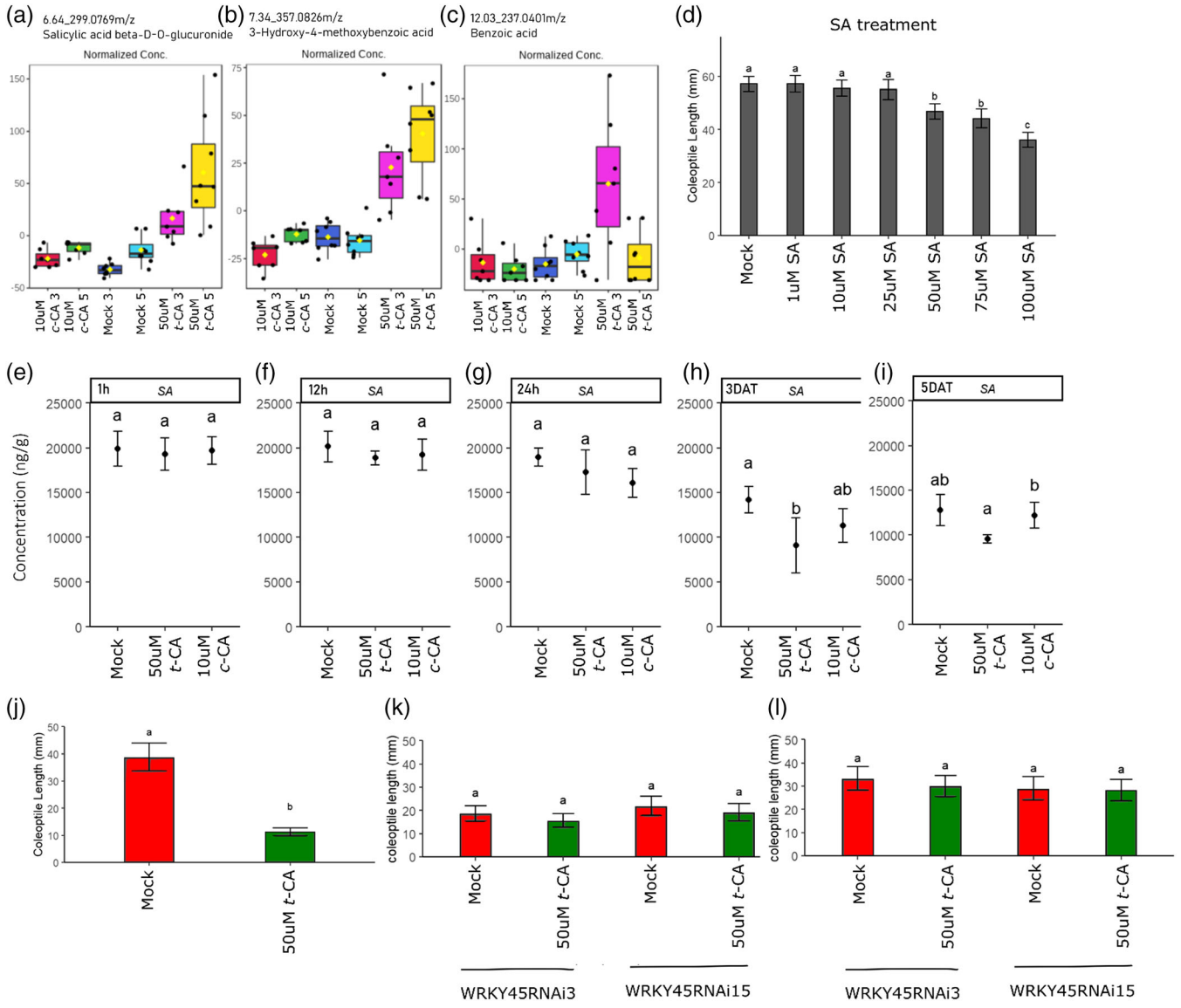

FIGURE 3 Possible link between *t*-CA treatment and SA. (a–c) abundance normalized for dry weight of salicylic acid beta-D-*O*-glucuronide (a), 3-hydroxy-4-methoxybenzoic acid (b) and benzoic acid (c) detected in an untargeted metabolomics experiment with coleoptiles treated with 10-μM *c*-CA, DMSO (mock) or 50-μM *t*-CA, and analyzed at 3 DAT (3) or 5 DAT (5). (d) Effect of 1-, 10-, 25-, 50-, 75-, and 100-μM SA treatment on coleoptile length at 5 DAT. (e-i) concentrations of SA after 1 (e), 12 (f), and 24 (g) h of 50-μM *t*-CA or 10-μM *c*-CA treatment and at 3 (h) and 5 (i) DAT. (j) Effect of 50-μM *t*-CA treatment on wild-type Nipponbare coleoptile lengths at 3 DAT. (k-l) effect of 50-μM *t*-CA treatment on coleoptile lengths of two Nipponbare WRKY45 RNAi lines at 3 (k) and 8 (l) DAT. Different letters indicate statistically significant differences at $p < 0.05$ ($n \geq 30$ in D, $n = 5$ in E–I, $n \geq 35$ in K; $n \geq 25$ in K, $n \geq 12$ in L).

3.4 | Next to *c*-CA also *t*-CA affects cell elongation via auxin regulation

The involvement of ATPases, the plethora of auxin-related differentially expressed genes upon *c*-CA treatment (Tables S2–S5), and the previous finding that *c*-CA can inhibit auxin efflux (Steenackers et al., 2017) prompted us to further examine the link between CA and auxin during coleoptile elongation. Primary auxin response genes, such as *Aux/IAA*, *SAUR*, and *ARF* (Sato et al., 2001; Steenackers et al., 2017), were more highly expressed in *c*-CA-treated coleoptiles as opposed to *t*-CA treatment where they seemed downregulated (Figure 4e). The transcriptome data also clearly indicated that genes involved in auxin metabolism and transport were also stimulated by *c*-CA treatment, whereas they were clearly downregulated upon *t*-CA treatment (Tables S2–S5). *GRETCHEN-HAAGEN 3.2* (*GH3.2*), an auxin-inducible gene involved in auxin conjugation, was strongly and steadily upregulated upon *c*-CA treatment, even as early as 1 h after treatment, whereas it was downregulated upon *t*-CA treatment (Figure 4d). Moreover, ATPase activity was found as a molecular process downregulated upon *t*-CA treatment (Figure S4). There was however no significant difference in H^+-ATPase activity between *t*-CA- and DMSO-treated coleoptiles at the 5% significance level

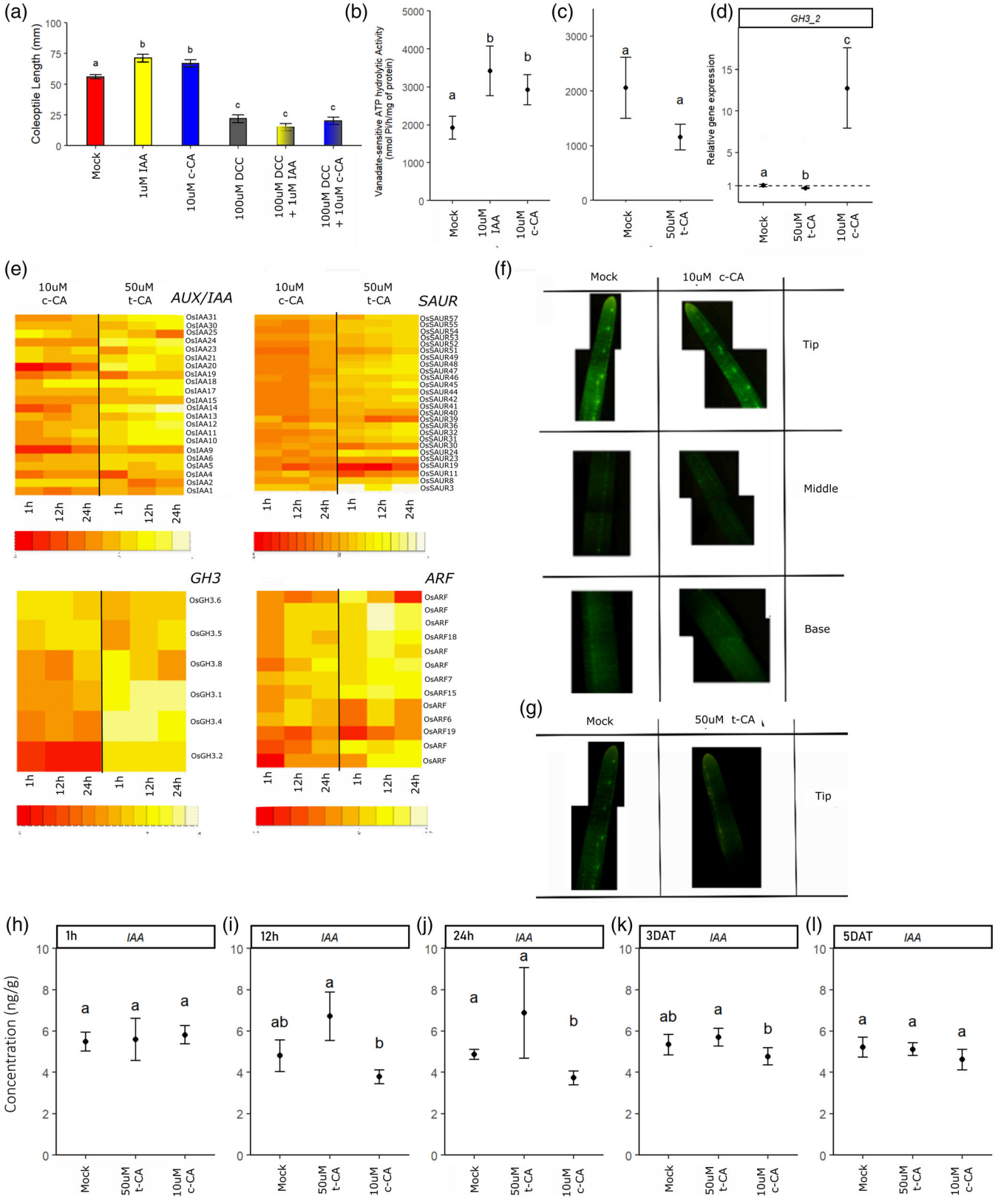

FIGURE 4 Legend on next page.

FIGURE 4 Linking auxin to *c*-CA and *t*-CA phenotypes. (a) Effect of 100-μM DCC and 100-μM DCC combined with 10-μM *c*-CA on coleoptile lengths at 5 DAT; 1-μM IAA and combined treatments with 1-μM IAA serve as a control. (b) Vanadate-sensitive ATP hydrolytic activity per 100 coleoptiles at 3 DAT for DMSO (mock), 10-μM IAA, or 10-μM *c*-CA-treated coleoptiles. (c) Vanadate-sensitive ATP hydrolytic activity per 100 coleoptiles at 3 DAT for DMSO (mock) or 50-μM *t*-CA-treated coleoptiles. (d) Relative expression of *GH3.2* after 1 h of treatment with 50-μM *t*-CA, 10-μM *c*-CA, or DMSO (mock). (e) Heatmap with significantly differently expressed members of the aux/IAA, SAUR, GH3, or ARF gene families. Note that the processed RNA sequencing results solely contain 50-μM *t*-CA and 10-μM *c*-CA treatment expression levels, which in fact represent the expression of *t*-CA and *c*-CA minus mock expression. (f) Tip, middle and base sections of DR5-VENUS coleoptiles 24 h after treatment with DMSO or 10-μM *c*-CA. (g) Tip sections of DR5-VENUS coleoptiles 24 h after treatment with DMSO or 50-μM *t*-CA. (h–l) Concentration of free IAA after 1 (h), 12 (i), and 24 (j) h of 50-μM *t*-CA or 10-μM *c*-CA treatment and at 3 (k) and 5 (l) DAT. Different letters indicate statistically significant differences at $p < 0.05$ ($n \geq 40$ in a, $n = 14$ in B, $n \geq 7$ in C, $n \geq 3$ in D, $n = 5$ in H–L).

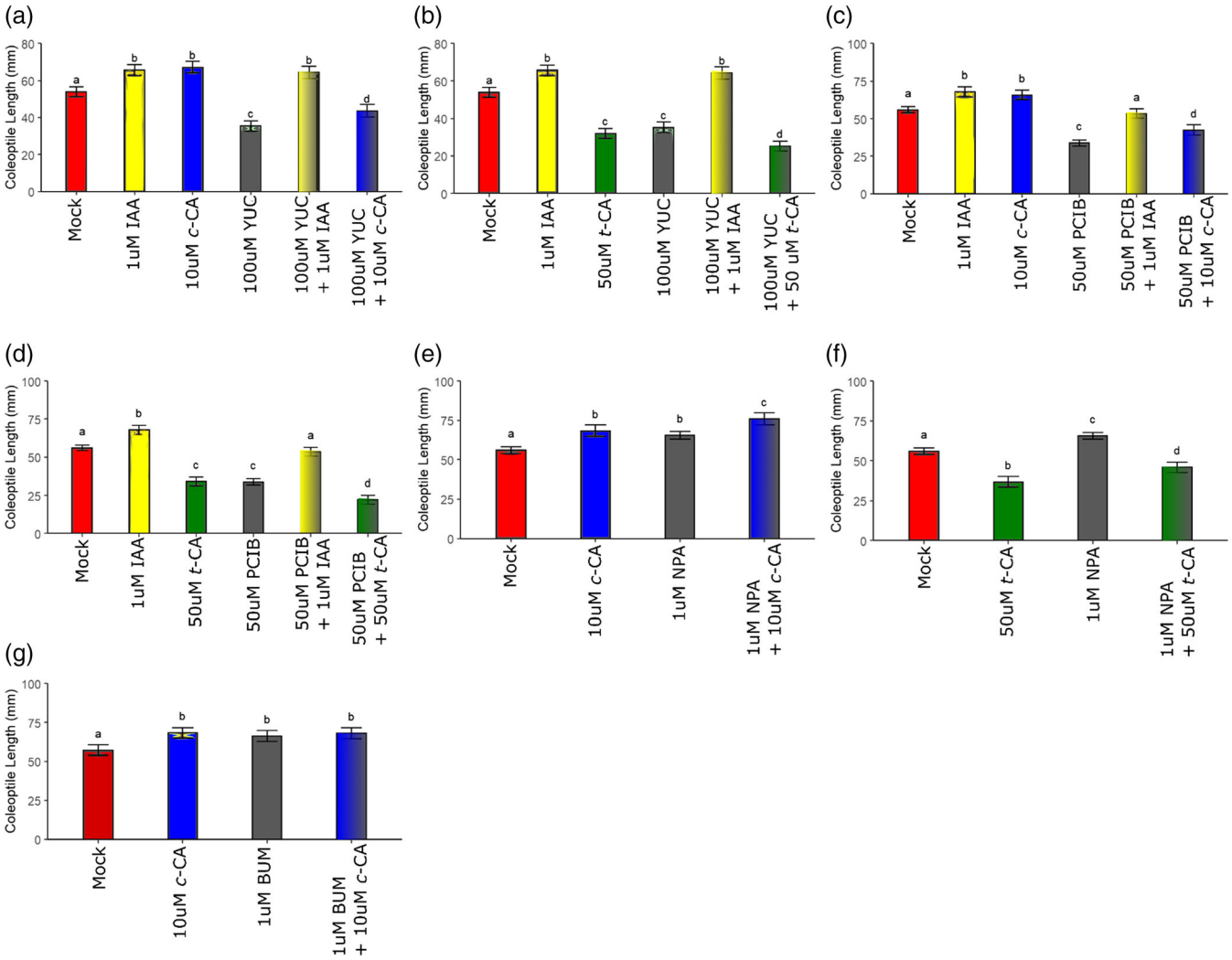

FIGURE 5 Effect of interference with auxin biosynthesis, transport, and perception. (a–b) effect of 100-μM yucasin treatment on 10-μM *c*-CA (a) and 50-μM *t*-CA (b)-dependent coleoptile elongation and inhibition, respectively. (c–d) Effect of 50-μM PCIB treatment on 10-μM *c*-CA (c) and 50-μM *t*-CA (d)-dependent coleoptile elongation and inhibition, respectively. (e–f) Effect of 1-μM NPA treatment on 10-μM *c*-CA (e) and 50-μM *t*-CA (f)-dependent coleoptile elongation and inhibition, respectively. (g) Effect of 1-μM BUM treatment on 10-μM *c*-CA dependent coleoptile elongation. Different letters indicate statistically significant differences at $p < 0.05$ ($n \geq 40$ in a, $n \geq 38$ in B–C and F–G, $n \geq 43$ in D, $n \geq 40$ in E).

($p = 0.05878$) (Figure 4c). When we measured free IAA levels in *c*-CA- or *t*-CA-treated coleoptiles (both for short-duration treatments as well as for longer treatments), the only significant difference, compared with DMSO-treated controls, was a decrease in free IAA levels at 24 h in *c*-CA-treated coleoptiles (Figure 4h-l). Also, a DR5-VENUS transgenic line that expresses an adjusted *YELLOW FLUORESCENT PROTEIN* (*YFP*) under control of the synthetic auxin-responsive promotor DR5rev (Yang et al., 2017) did not reveal a clear difference

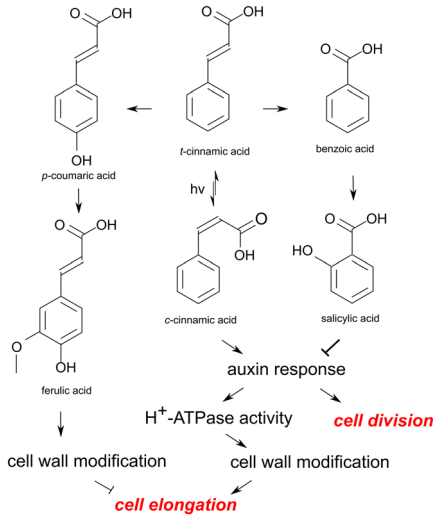

FIGURE 6 Model on the mode of action of *t*-CA-induced inhibition and *c*-CA-induced promotion of submerged rice coleoptile elongation, completed by transcriptional changes observed during CA treatment.

upon mock and *c*-CA treatment, although in both treatments a gradient was observed: the highest VENUS signal was clear in the tip, notably where auxin is synthesized, and where both the control and *c*-CA-treated coleoptiles are expanding (Figure 4f). There was only a weak signal in the DR5-VENUS lines in *t*-CA-treated coleoptiles, as compared with DMSO-treated controls (Figure 4g).

We further investigated the role of auxin biosynthesis, transport, and perception in CA-dependent coleoptile elongation using a pharmacological approach. When blocking auxin biosynthesis with yucasin (5-[4-chlorophenyl]-4H-1,2,4-triazole-3-thiol) (Nishimura et al., 2014), shorter coleoptiles were obtained. This could be restored by IAA treatment but not by *c*-CA treatment (Figure 5a). Co-treatment with yucasin and *t*-CA led to shorter coleoptile lengths as compared with *t*-CA and yucasin treatment alone (Figure 5b). These data indicate that the elongating and inhibiting effects of *c*-CA and *t*-CA, respectively, are possibly different from mere auxin biosynthesis effects.

Adding PCIB (2-[p-chlorophenoxy]-2-methylpropionic acid), an anti-auxin, also led to significantly shorter coleoptiles, which could be restored by IAA treatment or only partly when *c*-CA was added (Figure 5c). A combined treatment of PCIB with *t*-CA led to shorter coleoptile lengths as compared with *t*-CA or PCIB treatment alone, which induced similar coleoptile lengths (Figure 5d). Based on these findings, we conclude that the effects of CA isomers cannot be attributed to an interference with auxin perception.

Treatment with the auxin efflux inhibitor NPA (*N*-1-naphthylphthalamic acid) (Petrasek & Friml, 2009) led to significantly longer coleoptiles. Co-treatment with *c*-CA had an additive effect on coleoptile lengths (Figure 5e), whereas co-treatment with *t*-CA still resulted in longer coleoptiles in contrast to *t*-CA alone (Figure 5f). Also, treatment with BUM (2-(4-[diethylamino]-2-hydroxybenzoyl) benzoic acid), another auxin transport inhibitor that specifically inhibits ABCB-specific efflux (Kim et al., 2010), resulted in longer coleoptiles. But, as opposed to the NPA treatment, a co-treatment with *c*-CA had no additive effect on coleoptile lengths (Figure 5g). This could point toward the involvement of ABCB transporters in *c*-CA-mediated cell elongation.

4 | DISCUSSION AND CONCLUSION

The "acid growth theory," believed to be the key to cell expansion, states that auxin activates plasma membrane H^+-ATPases, resulting in proton efflux (Arsuffi & Braybrook, 2017). This in turn causes a drop in apoplastic pH that alters the activity of cell wall-modifying proteins (such as expansins, xyloglucan endotransglycosylase/hydrolases, and pectin methylesterases), which will mediate changes in cell wall extensibility. Additionally, the elevated plasma membrane H^+-ATPase activity hyperpolarizes the plasma membrane. This causes an increase in energy for solute uptake by activating K^+ channels and energizing H^+-coupled anion symporters, necessary to maintain water uptake and thus the turgor pressure that forces cell wall expansion (Du et al., 2020).

The observations that *c*-CA and *t*-CA stimulate and restrict cell elongation in submerged rice coleoptiles, respectively, prompted us to examine the underlying mechanistic processes with a specific focus on the link with the acid growth theory. A combination of transcriptomics, (untargeted) metabolomics, and pharmacological experiments with activity assays and genetic analyses led us to indeed propose a model in which *c*-CA activates proton pumps in the plasma membrane. This will ultimately result in localized cell elongation, possibly by interfering with auxin transport locally (notably in the coleoptile tip, where auxin levels and relative cell growth rate are the highest [Hoson et al., 1992; Narsai et al., 2015]). It has been previously reported in Arabidopsis that *c*-CA is a potent auxin efflux inhibitor capable of modifying local changes in auxin accumulation while not affecting overall auxin concentrations (Steenackers et al., 2017; Wasano et al., 2013). In line with this model, no consistent overall change in auxin concentration was found upon *c*-CA treatment of rice coleoptiles, whereas a rapid, significant, and consistent increase in the expression of primary auxin response genes was detected. Moreover, the stimulation of ATPase activity (and subsequent cell wall relaxation processes), ultimately leading to cell elongation upon *c*-CA treatment, was demonstrated and confirmed the link with local changes in the auxin landscape.

In contrast to the *c*-CA response, *t*-CA treatment resulted in a clear downregulation of genes involved in auxin metabolism and signaling. In agreement, a lower ATPase activity upon *t*-CA treatment previously has been demonstrated (Abenavoli et al., 2010; Lupini et al., 2016), and a negative effect of *t*-CA on cell elongation was also not unknown (Nagao & Ohwaki, 1955). Although our data did not unequivocally prove the involvement of H^+-ATPases during the restriction of cell growth by *t*-CA, we have found that *t*-CA impacts SA metabolism. Since SA can work antagonistically to auxin (Iglesias

et al., 2011), potentially mediated by GH3.5 (Dong et al., 2020; Westfall et al., 2016), this might explain the *t*-CA-induced inhibition of elongation. Indeed, benzoic acid and SA derivatives accumulated in *t*-CA-treated coleoptiles (similarly as reported in maize leaves, Araniti et al., 2018) and SA treatment led to the inhibition of coleoptile growth. An accumulation of free SA upon *t*-CA treatment could not be demonstrated, but rice shoots already have very high endogenous SA levels, and the increased accumulation of SA derivatives is a known mechanism to keep free SA levels under control. Recently, Tan et al. (2020) directly linked SA to auxin and growth attenuation in Arabidopsis through the direct binding of SA to the A-subunits of protein phosphatase 2A (PP2A), inhibiting the activity of this complex. This causes the hyperpolarization of the PIN2 auxin transporter, resulting in growth inhibition. In our RNA-seq dataset, several genes coding for a regulatory subunit of PP2A (i.e., LOC_Os06g37660, LOC_Os12g04290, LOC_Os11g04520, LOC_Os10g27050, and LOC_Os03g59060) were significantly differentially expressed upon *t*-CA treatment, whereas no difference was found upon *c*-CA treatment, making a direct link between *t*-CA and auxin plausible via SA signaling. Moreover, the inhibitory effect of *t*-CA treatment was lost in *WRKY45* RNAi lines. WRKY45 is a transcription factor induced by SA (Shimono et al., 2007) that regulates and controls the expression of phenylpropanoid genes (Akagi et al., 2014; Mutuku et al., 2019; Tao et al., 2009; Vicheka et al., 2017), which likely impacts cell elongation at the level of the cell wall.

t-CA can also directly affect cell wall rigidity by increasing feruloylation. FA is situated downstream of *t*-CA in the phenylpropanoid pathway and can cross-link different arabinoxylan molecules via FA bridges in the cell wall of grasses (Buanafina, 2009; Mnich et al., 2020; Tan et al., 1991). Indeed, the downregulation of four putative AFT genes reduces the ester-linked FA content in rice cell walls (Piston et al., 2010). Tan et al. (1991) demonstrated a negative correlation between cell wall extensibility and the content of FA mono- and dimers in cell walls of rice coleoptiles grown under water and in air. Moreover, Ishii and Saka (1992) found an inhibition of auxin-stimulated elongation of cells in rice lamina joints by feruloylated arabinoxylan trisaccharide, indicating that indeed, feruloylation of the cell wall can counteract rapid auxin-mediated cell expansion. Here, we observed a significantly higher expression of putative AFT genes, important in the process of feruloylation, in *t*-CA-treated rice coleoptiles. We also found a higher abundance of esterified FA and FA dimers in the cell wall of rice coleoptiles treated with *t*-CA, among others.

Besides an effect on elongation, there was a difference in total cell number upon the different treatments: *c*-CA-treated coleoptiles had on average a higher, and *t*-CA-treated had a lower cell number, compared with the control. The occurrence of cell divisions in submerged rice coleoptiles has been controversial but a recent study supports our findings, by showing that auxin signaling is involved in the cell division and tropism of submerged rice coleoptiles (Wu & Yang, 2020). This potential effect of *t*-CA and *c*-CA on cell division should be investigated further and should be linked to the proposed model (Chen, 2001; Perrot-Rechenmann, 2010).

Taken together, the obtained data support a model (Figure 6) in which *c*-CA treatment causes elongation in the submerged rice coleoptile due to an auxin response. This is potentially caused by the inhibition of auxin transport causing a local accumulation of auxin in the coleoptile tip. Subsequently, proton pumps are activated in the plasma membrane and acidification of the apoplast leads to cell wall modifications, eventually leading to cell elongation. *t*-CA, on the other hand, inhibits submerged rice coleoptile elongation. *t*-CA can be channeled into the phenylpropanoid pathway leading to FA and potentially other phenolic compounds that are built-in into the cell wall, causing cell rigidity. However, also, a link with SA is plausible, with a potential antagonistic mechanism with auxin signaling.

ACKNOWLEDGMENTS

We thank Breght Van den Berghe and Stan Van Praet for statistical advice during data analysis and Annick Bleys for her help in preparing the manuscript. We thank Lieven Sterck, Tom Van Hautegem, Boris Parizot, Heike Sprenger, and Julie Pevernagie for their help and insights during the analysis of the RNA sequencing data and also Steven Vandersyppe for his help during the LC–MS runs. This research was supported by Ghent University ("Bijzonder Onderzoeksfonds Methusalem project" no. BOF08/01M00408). L.V. is indebted to the Ghent University "Bijzonder Onderzoeksfonds" for a PhD fellowship (BOF01D28016).

CONFLICTS OF INTEREST

The authors declare that there are no conflicts of interest.

AUTHOR CONTRIBUTIONS

Lena Vlaminck, Bartel Vanholme, and Stephen Depuydt conceptualized and designed the experiments. Lena Vlaminck performed the experiments and analyzed the data. Lena Vlaminck, Bartel Vanholme, and Stephen Depuydt interpreted the data. Lena Vlaminck drafted the manuscript and Bartel Vanholme and Stephen Depuydt revised it. Brix De Rouck performed the cellular measurements of the whole coleoptile. Geert Goeminne ran the metabolomics and the hydroxycinnamic acid experiment samples, and Sandrien Desmet analyzed the output of the hydroxycinnamic acid experiment samples. Lien De Smet performed the extraction of the samples for hormonal measurements. Kristof Demeestere ran the hormone measurements, and Tina Kyndt analyzed the output. Veronique Storme did the statistical analysis on the RNA sequencing data, and Thijs Van Gerrewey performed the WGCNA analysis on the RNA sequencing results. Godelieve Gheysen and Dirk Inzé critically reviewed the manuscript. All authors read and approved the final manuscript.

DATA AVAILABILITY STATEMENT

The data that support the findings of this study are available on request from Lena Vlaminck or Stephen Depuydt.

ORCID

Lena Vlaminck https://orcid.org/0000-0002-0563-6492
Brix De Rouck https://orcid.org/0000-0002-8531-5313

Sandrien Desmet https://orcid.org/0000-0002-0957-708X
Thijs Van Gerrewey https://orcid.org/0000-0001-8913-4803
Geert Goeminne https://orcid.org/0000-0002-0337-2999
Lien De Smet https://orcid.org/0000-0002-0698-558X
Veronique Storme https://orcid.org/0000-0003-4762-6580
Tina Kyndt https://orcid.org/0000-0002-5267-5013
Kristof Demeestere https://orcid.org/0000-0003-3514-6045
Godelieve Gheysen https://orcid.org/0000-0003-1929-5059
Dirk Inzé https://orcid.org/0000-0002-3217-8407
Bartel Vanholme https://orcid.org/0000-0002-7214-7170
Stephen Depuydt https://orcid.org/0000-0001-8965-1026

REFERENCES

Abenavoli, M. R., Lupini, A., Oliva, S., & Sorgona, A. (2010). Allelochemical effects on net nitrate uptake and plasma membrane H^+-ATPase activity in maize seedlings. *Biologia Plantarum*, *54*, 149–153. https://doi.org/10.1007/s10535-010-0024-0

Abenavoli, M. R., Nicolo, A., Lupini, A., Oliva, S., & Sorgona, A. (2008). Effects of different allelochemicals on root morphology of *Arabidopsis thaliana*. *Allelopathy Journal*, *22*, 245–252.

Agati, G., Azzarello, E., Pollastri, S., & Tattini, M. (2012). Flavonoids as antioxidants in plants: Location and functional significance. *Plant Science*, *196*, 67–76. https://doi.org/10.1016/j.plantsci.2012.07.014

Akagi, A., Fukushima, S., Okada, K., Jiang, C.-J., Yoshida, R., Nakayama, A., Shimono, M., Sugano, S., Yamane, H., & Takatsuji, H. (2014). WRKY45-dependent priming of diterpenoid phytoalexin biosynthesis in rice and the role of cytokinin in triggering the reaction. *Plant Molecular Biology*, *86*, 171–183. https://doi.org/10.1007/s11103-014-0221-x

Araniti, F., Lupini, A., Mauceri, A., Zumbo, A., Sunseri, F., & Abenavoli, M. R. (2018). The allelochemical *trans*-cinnamic acid stimulates salicylic acid production and galactose pathway in maize leaves: A potential mechanism of stress tolerance. *Plant Physiology and Biochemistry*, *128*, 32–40. https://doi.org/10.1016/j.plaphy.2018.05.006

Arsuffi, G., & Braybrook, S. A. (2017). Acid growth: An ongoing trip. *Journal of Experimental Botany*, *69*, 137–146. https://doi.org/10.1093/jxb/erx390

Audus, L. J. (1972). *Plant growth substances*. Vol. 1: Chemistry and Physiology, Leonard Hill, London.

Bartley, L. E., Peck, M. L., Kim, S.-R., Ebert, B., Manisseri, C., Chiniquy, D. M., Sykes, R., Gao, L., Ruatengarten, C., Vega-Sanchez, M. E., Benke, P. I., Canlas, P. E., Cao, P., Brewer, S., Lin, F., Smith, W. L., Zhang, X., Keasling, J. D., Jentoff, R. E., … Ronald, P. C. (2013). Overexpression of a BAHD acyltransferase, OsAt10, alters rice cell wall hydroxycinnamic acid content and saccharification. *Plant Physiology*, *161*, 1615–1633. https://doi.org/10.1104/pp.112.208694

Benjamini, Y., & Hochberg, Y. (1995). Controlling the false discovery rate: A practical and powerful approach to multiple testing. *Journal of the Royal Statistical Society, Series B*, *57*, 289–300. https://doi.org/10.1111/j.2517-6161.1995.tb02031.x

Bernstein, H. I., & Quimby, W. C. (1943). The photochemical dimerization of *trans*-cinnamic acid. *Journal of the American Chemical Society*, *65*, 1845–1846. https://doi.org/10.1021/ja01250a016

Biała, W., & Jasiński, M. (2018). The phenylpropanoid case—It is transport that matters. *Frontiers in Plant Science*, *9*, 1610. https://doi.org/10.3389/fpls.2018.01610

Bolger, A. M., Lohse, M., & Usadel, B. (2014). Trimmomatic: A flexible trimmer for Illumina sequence data. *Bioinformatics*, *30*, 2114–2120. https://doi.org/10.1093/bioinformatics/btu170

Buanafina, M. M. (2009). Feruloylation in grasses: Current and future perspectives. *Molecular Plant*, *2*, 861–872. https://doi.org/10.1093/mp/ssp067

Chabannes, M., Ruel, K., Yoshinaga, A., Chabbert, B., Jauneau, A., Joseleau, J.-P., & Boudet, A.-M. (2001). In situ analysis of lignins in transgenic tobacco reveals a differential impact of individual transformations on the spatial patterns of lignin deposition at the cellular and subcellular levels. *The Plant Journal*, *28*, 271–282. https://doi.org/10.1046/j.1365-313X.2001.01159.x

Chen, J.-G. (2001). Dual auxin signaling pathways control cell elongation and division. *The Journal of Plant Growth Regulation*, *20*, 255–264. https://doi.org/10.1007/s003440010028

Clemens, S., & Weber, M. (2016). The essential role of coumarin secretion for Fe acquisition from alkaline soil. *Plant Signaling & Behavior*, *11*, e1114197. https://doi.org/10.1080/15592324.2015.1114197

Dong, C.-J., Liu, X.-Y., Xie, L.-L., Wang, L.-L., & Shang, Q.-M. (2020). Salicylic acid regulates adventitious root formation via competitive inhibition of the auxin conjugation enzyme CsGH3.5 in cucumber hypocotyls. *Planta*, *252*, 1–15. https://doi.org/10.1007/s00425-020-03403-4

Du, M., Spalding, E. P., & Gray, W. M. (2020). Rapid auxin-mediated cell expansion. *Annual Review of Plant Biology*, *71*, 1–24. https://doi.org/10.1146/annurev-arplant-073019-025907

El Houari, I., Van Beirs, C., Arents, H. E., Han, H., Chanoca, A., Opendacker, D., Pollier, J., Storme, V., Steenackers, W., Quareshy, M., Napier, R., Beeckman, T., Friml, J., De Rybel, B., Boerjan, W., & Vanholme, B. (2021). Seedling developmental defects upon blocking CINNAMATE-4-HYDROXYLASE are caused by perturbations in auxin transport. *New Phytologist*, *230*, 2275–2291. https://doi.org/10.1111/nph.17349

Fraser, C. M., & Chapple, C. (2011). The phenylpropanoid pathway in Arabidopsis. *The Arabidopsis Book*, *9*, e0152. https://doi.org/10.1199/tab.0152

Fujita, K., & Kubo, I. (2003). Synergism of polygodial and *trans*-cinnamic acid on inhibition of root elongation in lettuce seedling growth bioassays. *Journal of Chemical Ecology*, *29*, 2253–2262. https://doi.org/10.1023/A:1026270329989

Guaadaoui, A., Benaicha, S., Elmajdoub, N., Bellaoui, M., & Hamal, A. (2014). What is a bioactive compound? A combined definition for a preliminary consensus. *International Journal of Food Sciences and Nutrition*, *3*, 174–179. https://doi.org/10.11648/j.ijnfs.20140303.16

Haagen-Smit, A. J., & Went, F. W. (1935). A physiological analysis of the growth substance. *Proceedings of the Royal Academy of Sciences at Amsterdam*, *38*, 852–857.

Haeck, A., Van Langenhove, H., Harinck, L., Kyndt, T., Gheysen, G., Höfte, M., & Demeestere, K. (2018). Trace analysis of multi-class phytohormones in *Oryza sativa* using different scan modes in high-resolution orbitrap mass spectrometry: Method validation, concentration levels, and screening in multiple accessions. *Analytical and Bioanalytical Chemistry*, *410*, 4527–4539. https://doi.org/10.1007/s00216-018-1112-9

Hitchcock, A. E. (1935). Indole-3-n-propionic acid as a growth hormone and quantitative measurements of plant response. *Contributions from Boyce Thompson Institute*, *7*, 87–95.

Hollander, M., & Wolfe, D. A. (1973). *Nonparametric statistical methods* (Second ed.). John Wiley and Sons, Inc.

Hoson, T., Masuda, Y., & Pilet, P. E. (1992). Auxin content in Air and Water Grown Rice Coleoptiles. *Journal of Plant Physiology*, *139*(6), 685–689. https://doi.org/10.1016/s0176-1617(11)81711-6

Hsu, S.-K., & Tung, C.-W. (2017). RNA-seq analysis of diverse rice genotypes to identify the genes controlling coleoptile growth during submerged germination. *Frontiers in Plant Science*, *8*, 762.

Iglesias, M. J., Terrile, M. C., & Casalongué, C. A. (2011). Auxin and salicylic acid signalings counteract the regulation of adaptive responses to stress. *Plant Signaling & Behavior*, *6*, 452–454. https://doi.org/10.4161/psb.6.3.14676

Ishii, T., & Saka, H. (1992). Inhibition of auxin-stimulated elongation of cells in rice lamina joints by a feruloylated arabinoxylan trisaccharide. *Plant and Cell Physiology*, *33*, 321–324. https://doi.org/10.1093/oxfordjournals.pcp.a078257

Jain, M., Nijhawan, A., Tyagi, A. K., & Khurana, J. P. (2006). Validation of housekeeping genes as internal control for studying gene expression in rice by quantitative real-time PCR. *Biochemical and Biophysical Research Communications*, *345*, 646–651. https://doi.org/10.1016/j.bbrc.2006.04.140

Jones, L., Ennos, A. R., & Turner, S. R. (2001). Cloning and characterization of irregular Xylem4 (Irx4): A severe lignin-deficient mutant of Arabidopsis. *The Plant Journal*, *26*, 205–216. https://doi.org/10.1046/j.1365-313x.2001.01021.x

Kim, J. Y., Henrichs, S., Bailly, A., Vincenzetti, V., Sovero, V., Mancuso, S., Pollmann, S., Kim, D., Geisler, M., & Nam, H. G. (2010). Identification of an ABCB/P-glycoprotein-specific inhibitor of auxin transport by chemical genomics. *Journal of Biological Chemistry*, *285*, 23309–23317. https://doi.org/10.1074/jbc.M110.105981

Kinoshita, T., Nishimura, M., & Shimazaki, K. (1995). Cytosolic concentration of Ca2+ regulates the plasma membrane H^+-ATPase in guard cells of fava bean. *The Plant Cell*, *7*, 1333–1342. https://doi.org/10.2307/3870106

Köhl, K. (2015). Growing rice in controlled environments. *Annals of Applied Biology*, *167*, 157–177. https://doi.org/10.1111/aab.12220

Kumar, D., Das, P. K., & Sarmah, B. K. (2018). Reference gene validation for normalization of RT-qPCR assay associated with germination and survival of rice under hypoxic condition. *Journal of Applied Genetics*, *59*, 419–430. https://doi.org/10.1007/s13353-018-0466-1

Kurepa, J., Shull, T. E., Karunadasa, S. S., & Smalle, J. A. (2018). Modulation of auxin and cytokinin responses by early steps of the phenylpropanoid pathway. *BMC Plant Biology*, *18*, 1, 278–15. https://doi.org/10.1186/s12870-018-1477-0

Langfelder, P., & Horvath, S. (2008). WGCNA: An R package for weighted correlation network analysis. *BMC Bioinformatics*, *9*, 559. https://doi.org/10.1186/1471-2105-9-559

Lefevere, H., Bauters, L., & Gheysen, G. (2020). Salicylic acid biosynthesis in plants. *Frontiers in Plant Science*, *11*(April), 1–7.

Letham, D. S., Goodwin, P. B., & Higgins, T. J. V. (1978). Naturally occurring plant growth regulators other than the principle hormones of higher plants. In D. S. Letham, P. B. Goodwin, & T. J. V. Higgins (Eds.), *Phytohormones and relative compounds: A comprehensive treatise* (Vol. 1) (pp. 349–417). Elsevier/North Holland Biomedical Press.

Li, H.-H., Inoue, M., Nishimura, H., Mizutani, J., & Tsuzuki, E. (1993). Interactions of *trans*-cinnamic acid, its related phenolic allelochemicals, and abscisic acid in seedling growth and seed germination of lettuce. *Journal of Chemical Ecology*, *19*, 1775–1787. https://doi.org/10.1007/BF00982307

Li, X. (2020). Riceidconverter: Convert Biological ID from RAP or MSU to SYMBOL for *Oryza Sativa*. https://CRAN.R-project.org/package=riceidconverter

Li, Y. (2022). GO/KEGG enrichment analysis on gene Lists from Rice (*Oryza Sativa*). *Bio-101*, *12*, e4446. https://doi.org/10.21769/BioProtoc.4446

Liu, C.-W., & Murray, J. (2016). The role of flavonoids in nodulation host-range specificity: An update. *Plants*, *5*, 33. https://doi.org/10.3390/plants5030033

Livak, K. J., & Schmittgen, T. D. (2001). Analysis of relative gene expression data using real-time quantitative PCR and the $2-\Delta\Delta CT$ method. *Methods*, *25*, 402–408. https://doi.org/10.1006/meth.2001.1262

Lund, S. P., Nettleton, D., McCarthy, D. J., & Smyth, G. K. (2012). Detecting differential expression in RNA-sequence data using quasi-likelihood with shrunken dispersion estimates. *Statistical Applications in Genetics and Molecular Biology*, *11*, 1–42. https://doi.org/10.1515/1544-6115.1826

Lupini, A., Sorgonà, A., Princi, M. P., Sunseri, F., & Abenavoli, M. R. (2016). Morphological and physiological effects of *trans*-Cinnamic acid and its hydroxylated derivatives on maize root types. *Plant Growth Regulation*, *78*, 263–273. https://doi.org/10.1007/s10725-015-0091-5

Magneschi, L., Kudahettige, R. L., Alpi, A., & Perata, P. (2009). Expansin gene expression and anoxic coleoptile elongation in rice cultivars. *Journal of Plant Physiology*, *166*, 1576–1580. https://doi.org/10.1016/j.jplph.2009.03.008

Masuda, Y., & Tanimoto, E. (1967). Effect of auxin and antiauxin on the growth and RNA synthesis of etiolated pea internode. *Plant and Cell Physiology*, *8*, 459–465.

Mathesius, U. (2018). Flavonoid functions in plants and their interactions with other organisms. *Plants*, *7*, 30. https://doi.org/10.3390/plants7020030

Mnich, E., Bjarnholt, N., Eudes, A., Harholt, J., Holland, C., Jørgensen, B., Larsen, F. H., Liu, M., Manat, R., Meyer, A. S., Mikkelsen, J. D., Motawia, M. S., Muschiol, J., Moller, B. L., Moller, S. R., Perzon, A., Petersen, B. L., Ravn, J. L., & Ulvskov, P. (2020). Phenolic cross-links: Building and de-constructing the plant cell wall. *Natural Product Reports*, *37*, 919–961. https://doi.org/10.1039/C9NP00028C

Morris, D. A., & Arthur, E. D. (1984). Invertase and auxin-induced elongation in internodal segments of *Phaseolus Vulgaris*. *Phytochemistry*, *23*, 2163–2167. https://doi.org/10.1016/S0031-9422(00)80512-9

Mutuku, J. M., Cui, S., Hori, C., Takeda, Y., Tobimatsu, Y., Nakabayashi, R., Mori, T., Saito, K., Demura, T., Umezawa, T., Yoshida, S., & Shirasu, K. (2019). The structural integrity of lignin is crucial for resistance against *Striga hermonthica* parasitism in rice. *Plant Physiology*, *179*, 1796–1809. https://doi.org/10.1104/pp.18.01133

Nagao, M., & Ohwaki, Y. (1955). The action of *trans*-cinnamic acid and 2,3,5-triiodobenzoic acids in the rice seedling. *Science Report Tohoku University*, *21*, 96–108.

Naoumkina, M., Zhao, Q., Gallego-Giraldo, L., Dai, X., Zhao, P. X., & Dixon, R. A. (2010). Genome-wide analysis of phenylpropanoid defence pathways. *Molecular Plant Pathology*, *11*, 829–846. https://doi.org/10.1111/j.1364-3703.2010.00648.x

Narsai, R., Edwards, J. M., Roberts, T. H., Whelan, J., Joss, G. H., & Atwell, B. J. (2015). Mechanisms of growth and patterns of gene expression in oxygen-deprived rice coleoptiles. *The Plant Journal*, *82*, 25–40. https://doi.org/10.1111/tpj.12786

Nelissen, H., Rymen, B., Coppens, F., Dhondt, S., Fiorani, F., & Beemster, G. T. S. (2013). Kinematic analysis of cell division in leaves of mono- and dicotyledonous species: a basis for understanding growth and developing refined molecular sampling strategies. In I. De Smet (Ed.), *Plant organogenesis: Methods and protocols* (pp. 248–264). Springer Science and Business media, LLC. https://doi.org/10.1007/978-1-62703-221-6_17

Nelson, N., & Harvey, W. R. (1999). Vacuolar and plasma membrane proton-adenosine-triphosphatases. *Physiological Reviews*, *79*, 361–385. https://doi.org/10.1152/physrev.1999.79.2.361

Nishimura, T., Hayashi, K., Suzuki, H., Gyohda, A., Takaoka, C., Sakaguchi, Y., Matsumoto, S., Kasahara, H., Sakai, T., Kato, J.-I., Kamiya, Y., & Koshiba, T. (2014). Yucasin is a potent inhibitor of YUCCA, a key enzyme in auxin biosynthesis. *The Plant Journal*, *77*, 352–366. https://doi.org/10.1111/tpj.12399

Okumura, M., & Kinoshita, T. (2016). Measurement of ATP hydrolytic activity of plasma membrane H^+-ATPase from *Arabidopsis thaliana* leaves. *Bio-Protocol*, *6*, e2044.

Oliveros, J. C. (2015). Venny. An interactive tool for comparing lists with venn's diagrams. 2015.

Pan, L., Kawai, M., Yano, A., & Uchimiya, H. (2000). Nucleoside diphosphate kinase required for coleoptile elongation in rice. *Plant Physiology*, *122*, 447–452. https://doi.org/10.1104/pp.122.2.447

Perrot-Rechenmann, C. (2010). Cellular responses to auxin: division versus expansion. *Cold Spring Harbor Perspectives in Biology*, *2*, a001446.

Petrasek, J., & Friml, J. (2009). Auxin transport routes in plant development. *Development*, *136*, 2675–2688. https://doi.org/10.1242/dev.030353

Pfändler, R., Scheel, D., Sandermann, H. Jr., & Grisebach, H. (1977). Stereospecificity of plant microsomal cinnamic acid 4-hydroxylase. *Archives of Biochemistry and Biophysics*, *178*, 315–316. https://doi.org/10.1016/0003-9861(77)90197-7

Piston, F., Uauy, C., Fu, L., Langston, J., Labavitch, J., & Dubcovsky, J. (2010). Down-regulation of four putative arabinoxylan feruloyl transferase genes from family PF02458 reduces ester-linked ferulate content in rice cell walls. *Planta*, *231*, 677–691. https://doi.org/10.1007/s00425-009-1077-1

R core team. (2014). R: A language and environment for statistical computing. Vienna, Austria: R foundation for Statistical Computing. http://www.r-project.org/

Rivas-San Vicente, M., & Plasencia, J. (2011). Salicylic acid beyond defence: Its role in plant growth and development. *Journal of Experimental Botany*, *62*, 3321–3338. https://doi.org/10.1093/jxb/err031

Robinson, M. D., McCarthy, D. J., & Smyth, G. K. (2010). EdgeR: A bioconductor package for differential expression analysis of digital gene expression data. *Bioinformatics*, *26*, 139–140. https://doi.org/10.1093/bioinformatics/btp616

Robinson, M. D., & Oshlack, A. (2010). A scaling normalization method for differential expression analysis of RNA-seq data. *Genome Biology*, *11*, R25. https://doi.org/10.1186/gb-2010-11-3-r25

Sato, Y., Nishimura, A., Ito, M., Ashikari, M., Hirano, H. Y., & Matsuoka, M. (2001). Auxin response factor family in rice. *Genes & Genetic Systems*, *76*, 373–380. https://doi.org/10.1266/ggs.76.373

Schalk, M., Cabello-hurtado, F., Atanossova, R., & Saindrenan, P. (1998). Piperonylic acid, a selective, mechanism-based inactivator of the *trans*-cinnamate 4-hydroxylase: A new tool to control the flux of metabolites in the phenylpropanoid pathway. *Plant Physiology*, *118*, 209–218. https://doi.org/10.1104/pp.118.1.209

Shah, J. (2003). The salicylic acid loop in plant defense. *Current Opinion in Plant Biology*, *6*, 365–371. https://doi.org/10.1016/S1369-5266(03)00058-X

Shalaby, S., & Horwitz, B. A. (2015). Plant phenolic compounds and oxidative stress: Integrated signals in fungal–plant interactions. *Current Genetics*, *61*, 347–357. https://doi.org/10.1007/s00294-014-0458-6

Shimono, M., Sugano, S., Nakayama, A., Jiang, C.-J., Ono, K., Toki, S., & Takatsuji, H. (2007). Rice WRKY45 plays a crucial role in benzothiadiazole-inducible blast resistance. *The Plant Cell*, *19*, 2064–2076. https://doi.org/10.1105/tpc.106.046250

Steenackers, W., El Houari, I., Baekelandt, A., Witvrouw, K., Dhondt, S., Leroux, O., Gonzalez, N., Corneillie, S., Cesarino, I., Inzé, D., Boerjan, W., & Vanholme, B. (2019). *Cis*-cinnamic acid is a natural plant growth-promoting compound. *Journal of Experimental Botany*, *70*, 6293–6304. https://doi.org/10.1093/jxb/erz392

Steenackers, W., Klíma, P., Quareshy, M., Cesarino, I., Kumpf, R. P., Corneillie, S., Araújo, P., Viaene, T., Goeminne, G., Nowack, M. K., Ljung, K., Friml, J., Blakeslee, J. J., Novak, O., Zazimalova, E., Napier, R., Boerjan, W., & Vanholme, B. (2017). *Cis*-cinnamic acid is a novel, natural auxin efflux inhibitor that promotes lateral root formation. *Plant Physiology*, *173*, 552–565. https://doi.org/10.1104/pp.16.00943

Supek, F., Bošnjak, M., Škunca, N., & Šmuc, T. (2011). "REVIGO summarizes and visualizes long lists of gene ontology terms" ed. Cynthia Gibas. *PLoS ONE*, *6*, e21800. https://doi.org/10.1371/journal.pone.0021800

Tan, K.-S., Hoson, T., Masuda, Y., & Kamisaka, S. (1991). Correlation between cell wall extensibility and the content of diferulic and ferulic acids in cell walls of *Oryza sativa* coleoptiles grown under water and in air. *Physiologia Plantarum*, *83*, 397–403. https://doi.org/10.1111/j.1399-3054.1991.tb00111.x

Tan, S., Abas, M., Verstraeten, I., Glanc, M., Molnár, G., Hajný, J., Lasák, P., Petrik, I., Russinova, E., Petrasek, J., Novak, O., Pospisil, J., & Friml, J. (2020). Salicylic acid targets protein phosphatase 2A to attenuate growth in plants. *Current Biology*, *30*, 381–395.e8.

Tao, Z., Liu, H., Qiu, D., Zhou, Y., Li, X., Xu, C., & Wang, S. (2009). A pair of allelic WRKY genes play opposite roles in rice-bacteria interactions. *Plant Physiology*, *151*, 936–948. https://doi.org/10.1104/pp.109.145623

Thimm, O., Blasing, O., Gibon, Y., Nagel, A., Meyer, S., Kruger, P., Selbig, J., Muller, L. A., Rhee, S. Y., & Stitt, M. (2004). MAPMAN: A user-driven tool to display genomics data sets onto diagrams of metabolic pathways and other biological processes. *The Plant Journal*, *37*, 914–939. https://doi.org/10.1111/j.1365-313X.2004.02016.x

Van Bel, M., Diels, T., Vancaester, E., Kreft, L., Botzki, A., Van de Peer, Y., Coppens, F., & Vandepoele, K. (2018). PLAZA 4.0: An integrative resource for functional, evolutionary and comparative plant genomics. *Nucleic Acids Research*, *46*(D1), D1190–D1196. https://doi.org/10.1093/nar/gkx1002

Van Overbeek, J., Blondeau, R., & Horne, V. (1951). *Trans*-cinnamic acid as an anti-auxin. *American Journal of Botany*, *38*, 589–595. https://doi.org/10.1002/j.1537-2197.1951.tb14863.x

Vanholme, B., El Houari, I., & Boerjan, W. (2019). Bioactivity: phenylpropanoids' best kept secret. *Current Opinion in Biotechnology*, *56*, 156–162. https://doi.org/10.1016/j.copbio.2018.11.012

Vanholme, R., Storme, V., Vanholme, B., Sundin, L., Christensen, J. H., Goeminne, G., Halpin, C., Rohde, A., Morreel, K., & Boerjan, W. (2012). A systems biology view of responses to lignin biosynthesis perturbations in Arabidopsis. *The Plant Cell*, *24*, 3506–3529. https://doi.org/10.1105/tpc.112.102574

Veldstra, H. (1944). Researches on plant growth substances IV. Relation between chemical structure and physiological activity I. *Enzymologia*, *11*, 97–136.

Veldstra, H. (1953). The relation of chemical structure to biological activity in growth substances. *Annual Review of Plant Physiology*, *4*, 151–198. https://doi.org/10.1146/annurev.pp.04.060153.001055

Vicheka, T., Yun, S., Lindain, A. F., Sopheareth, M., Chung, I. K., & Kim, K. M. (2017). Defense gene expression and phenotypic changes of rice (*Oryza sativa* L.) at the reproductive stage in response to whitebacked planthopper (*Sogatella furcifera horvath*) infestation. *Cereal Research Communications*, *45*, 456–465. https://doi.org/10.1556/0806.45.2017.025

Vlaminck, L., Sang-Aram, C., Botterman, D., Uy, C., Harper, M. K., Inze, D., Gheysen, G., & Depuydt, S. (2020). Development of a novel and rapid phenotype-based screening method to assess rice seedling growth. *Plant Methods*, *16*, 1–19. https://doi.org/10.1186/s13007-020-00682-6

Vogt, T. (2010). Phenylpropanoid biosynthesis. *Molecular Plant*, *3*, 2–20. https://doi.org/10.1093/mp/ssp106

Wasano, N., Sugano, M., Nishikawa, K., Okuda, K., Shindo, M., Abe, H., Park, S.-Y., Hiradate, S., Kamo, T., & Fujii, Y. (2013). Root-specific induction of early auxin-responsive genes in *Arabidopsis thaliana* by *cis*-cinnamic acid. *Plant Biotechnology*, *30*, 465–471. https://doi.org/10.5511/plantbiotechnology.13.0718a

Westfall, C. S., Sherp, A. M., Zubieta, C., Alvarez, S., Schraft, E., Marcellin, R., Ramirez, L., & Jez, J. M. (2016). *Arabidopsis thaliana* GH3.5 acyl acid amido synthetase mediates metabolic crosstalk in auxin and salicylic acid homeostasis. *Proceedings of the National Academy of Sciences*, *113*, 13917–13922. https://doi.org/10.1073/pnas.1612635113

Wong, W. S., Guo, D., Wang, X. L., Yin, Z. Q., Xia, B., & Li, N. (2005). Study of *cis*-cinnamic acid in *Arabidopsis thaliana*. *Plant Physiology and Biochemistry*, *43*, 929–937. https://doi.org/10.1016/j.plaphy.2005.08.008

Wu, T., Hu, E., Xu, S., Chen, M., Guo, P., Dai, Z., Feng, T., Zhou, L., Tang, W., Zhan, L., Fu, X., Liu, S., Bo, X., & Yu, G. (2021). clusterProfiler 4.0: A universal enrichment tool for interpreting omics data. *The Innovation*, *2*(3), 100141. https://doi.org/10.1016/j.xinn.2021.100141

Wu, Y. S., & Yang, C. Y. (2020). Comprehensive transcriptomic analysis of auxin responses in submerged rice coleoptile growth. *International Journal of Molecular Sciences*, *21*, 1292. https://doi.org/10.3390/ijms21041292

Yang, J., Yuan, Z., Meng, Q., Huang, G., Périn, C., Bureau, C., Meunier, A.-C., Ingouff, M., Bennett, M. J., Liang, W., & Zhang, D. (2017). Dynamic regulation of auxin response during rice development revealed by newly established hormone biosensor markers. *Frontiers in Plant Science*, *8*, 256.

Yang, L., Wen, K.-S., Ruan, X., Zhao, Y.-X., Wei, F., & Wang, Q. (2018). Response of plant secondary metabolites to environmental factors. *Molecules*, *23*, 762. https://doi.org/10.3390/molecules23040762

Yang, X. X., Choi, H. W., Yang, S. F., & Li, N. (1999). A UV-light activated cinnamic acid isomer regulates plant growth and gravitropism via an ethylene receptor-independent pathway. *Australian Journal of Plant Physiology*, *26*, 325–335.

Yin, Z. Q., Wong, W., Ye, W., & Li, N. (2003). Biologically active *cis*-cinnamic acid occurs naturally in *Brassica parachinensis*. *Chinese Science Bulletin*, *48*, 555–558. https://doi.org/10.1360/03tb9118

SUPPORTING INFORMATION

Additional supporting information can be found online in the Supporting Information section at the end of this article.

How to cite this article: Vlaminck, L., De Rouck, B., Desmet, S., Van Gerrewey, T., Goeminne, G., De Smet, L., Storme, V., Kyndt, T., Demeestere, K., Gheysen, G., Inzé, D., Vanholme, B., & Depuydt, S. (2022). Opposing effects of *trans*- and *cis*-cinnamic acid during rice coleoptile elongation. *Plant Direct*, *6*(12), e465. https://doi.org/10.1002/pld3.465